

# Space is the Place: Effects of Continuous Spatial Structure on Analysis of Population Genetic Data

C.J. Battey<sup>\*,†</sup>, Peter L. Ralph<sup>\*,†</sup> and Andrew D. Kern<sup>\*,†</sup>

<sup>\*</sup>University of Oregon Dept. Biology, Institute for Ecology Evolution

**ABSTRACT** Real geography is continuous, but standard models in population genetics are based on discrete, well-mixed populations. As a result many methods of analyzing genetic data assume that samples are a random draw from a well-mixed population, but are applied to clustered samples from populations that are structured clinally over space. Here we use simulations of populations living in continuous geography to study the impacts of dispersal and sampling strategy on population genetic summary statistics, demographic inference, and genome-wide association studies. We find that most common summary statistics have distributions that differ substantially from that seen in well-mixed populations, especially when Wright's neighborhood size is less than 100 and sampling is spatially clustered. Stepping-stone models reproduce some of these effects, but discretizing the landscape introduces artifacts which in some cases are exacerbated at higher resolutions. The combination of low dispersal and clustered sampling causes demographic inference from the site frequency spectrum to infer more turbulent demographic histories, but averaged results across multiple simulations revealed surprisingly little systematic bias. We also show that the combination of spatially autocorrelated environments and limited dispersal causes genome-wide association studies to identify spurious signals of genetic association with purely environmentally determined phenotypes, and that this bias is only partially corrected by regressing out principal components of ancestry. Last, we discuss the relevance of our simulation results for inference from genetic variation in real organisms.

**KEYWORDS** Space; Population Structure; Demography; Haplotype block sharing; GWAS

## Introduction

The inescapable reality that biological organisms live, move, and reproduce in continuous geography is usually omitted from population genetic models. However, mates tend to live near to one another and to their offspring, leading to a positive correlation between genetic differentiation and geographic distance. This pattern of “isolation by distance” (Wright 1943) is one of the most widely replicated empirical findings in population genetics (Aguillon *et al.* 2017; Jay *et al.* 2012; Sharbel *et al.* 2000). Despite a long history of analytical work describing the genetics of populations distributed across continuous geography (e.g., Wright (1943); Rousset (1997); Barton *et al.* (2002, 2010); Ringbauer *et al.* (2017); Robledo-Arnuncio and Rousset (2010); Wilkins and Wakeley (2002); Wilkins (2004)), much modern work still describes geographic structure as a set of discrete populations connected by migration (e.g., Wright 1931; Epperson 2003; Rousset and Leblois 2011; Shirk and Cushman 2014; Lundgren and Ralph 2019)

Manuscript compiled: Friday 20<sup>th</sup> March, 2020

<sup>†</sup>301 Pacific Hall, University of Oregon Dept. Biology, Institute for Ecology and Evolution. cbattey2@uoregon.edu.

<sup>†</sup>these authors co-supervised this project

39 or as an average over such discrete models (Petkova *et al.* 2015; Al-Asadi *et al.* 2019). For this reason,  
40 most population genetics statistics are interpreted with reference to discrete, well-mixed populations,  
41 and most empirical papers analyze variation within clusters of genetic variation inferred by programs  
42 like *STRUCTURE* (Pritchard *et al.* 2000) with methods that assume these are randomly mating units.

43 The assumption that populations are “well-mixed” has important implications for downstream  
44 inference of selection and demography. Methods based on the coalescent (Kingman 1982; Wakeley  
45 2009) assume that the sampled individuals are a random draw from a well-mixed population that is  
46 much larger than the sample (Wakeley and Takahashi 2003). The key assumption is that the individuals  
47 of each generation are *exchangeable*, so that there is no correlation between the fate or fecundity of a  
48 parent and that of their offspring (Huillet and Möhle 2011). If dispersal or mate selection is limited by  
49 geographic proximity, this assumption can be violated in many ways. For instance, if mean viability or  
50 fecundity is spatially autocorrelated, then limited geographic dispersal will lead to parent–offspring  
51 correlations. Furthermore, nearby individuals will be more closely related than an average random  
52 pair, so drawing multiple samples from the same area of the landscape will represent a biased sample  
53 of the genetic variation present in the whole population (Städler *et al.* 2009).

54 Two areas in which spatial structure may be particularly important are demographic inference and  
55 genome-wide association studies (GWAS). Previous work has found that discrete population structure  
56 can create false signatures of population bottlenecks when attempting to infer demographic histories  
57 from microsatellite variation (Chikhi *et al.* 2010), statistics summarizing the site frequency spectrum  
58 (SFS) (Ptak and Przeworski 2002; Städler *et al.* 2009; St. Onge *et al.* 2012), or runs of homozygosity in a  
59 single individual (Mazet *et al.* 2015). The increasing availability of whole-genome data has led to the  
60 development of many methods that attempt to infer detailed trajectories of population sizes through  
61 time based on a variety of summaries of genetic data (Liu and Fu 2015; Schiffels and Durbin 2014;  
62 Sheehan *et al.* 2013; Terhorst *et al.* 2016). Because all of these methods assume that the populations  
63 being modeled are approximately randomly mating, they are likely affected by spatial biases in the  
64 genealogy of sampled individuals (Wakeley 1999), which may lead to incorrect inference of population  
65 changes over time (Mazet *et al.* 2015). However, previous investigations of these effects have focused on  
66 discrete rather than continuous space models, and the level of isolation by distance at which inference  
67 of population size trajectories become biased by structure is not well known. Here we test how two  
68 methods suitable for use with large samples of individuals – stairwayplot (Liu and Fu 2015) and  
69 SMC++ (Terhorst *et al.* 2016) – perform when applied to populations evolving in continuous space  
70 with varying sampling strategies and levels of dispersal.

71 Spatial structure is also a major challenge for interpreting the results of genome-wide association  
72 studies (GWAS). This is because many phenotypes of interest have strong geographic differences due  
73 to the (nongenetic) influence of environmental or socioeconomic factors, which can therefore show  
74 spurious correlations with spatially patterned allele frequencies (Bulik-Sullivan *et al.* 2015; Mathieson  
75 and McVean 2012). Indeed, two recent studies found that previous evidence of polygenic selection on  
76 human height in Europe was confounded by subtle population structure (Sohail *et al.* 2018; Berg *et al.*  
77 2018), suggesting that existing methods to correct for population structure in GWAS are insufficient.  
78 However we have little quantitative idea of the population and environmental parameters that can be  
79 expected to lead to biases in GWAS.

80 Last, some of the most basic tools of population genetics are summary statistics like  $F_{IS}$  and  
81 Tajima’s  $D$ , which are often interpreted as reflecting the influence of selection or demography on  
82 sampled populations (Tajima 1989). Statistics like Tajima’s  $D$  are essentially summaries of the site  
83 frequency spectrum, which itself reflects variation in branch lengths and tree structure of the underlying  
84 genealogies of sampled individuals. Geographically limited mate choice distorts the distribution of  
85 these genealogies (Maruyama 1972; Wakeley 1999), which can affect the value of Tajima’s  $D$  (Städler  
86 *et al.* 2009). Similarly, the distribution of tract lengths of identity by state among individuals contains  
87 information about not only historical demography (Harris and Nielsen 2013; Ralph and Coop 2013)  
88 and selection (Garud *et al.* 2015), but also dispersal and mate choice (Ringbauer *et al.* 2017; Baharian  
89 *et al.* 2016). We are particularly keen to examine how such summaries will be affected by models that  
90 incorporate continuous space, both to evaluate the assumptions underlying existing methods and to  
91 identify where the most promising signals of geography lie.

92 To study this, we have implemented an individual-based model in continuous geography that  
93 incorporates overlapping generations, local dispersal of offspring, and density-dependent survival. We  
94 simulate chromosome-scale genomic data in tens of thousands of individuals from parameter regimes  
95 relevant to common subjects of population genetic investigation, and output the full genealogy and  
96 recombination history of all final-generation individuals. We use these simulations to test how sampling  
97 strategy interacts with geographic population structure to cause systematic variation in population  
98 genetic summary statistics typically analyzed assuming discrete population models. We then examine  
99 how the fine-scale spatial structures occurring under limited dispersal impact demographic inference  
100 from the site frequency spectrum. Last, we examine the impacts of continuous geography on genome-  
101 wide association studies (GWAS) and identify regions of parameter space under which the results from  
102 GWAS may be misleading.

## 103 Materials and Methods

### 104 *Modeling Evolution in Continuous Space*

105 The degree to which genetic relationships are geographically correlated depends on the chance that  
106 two geographically nearby individuals are close relatives – in modern terms, by the tension between  
107 migration (the chance that one is descended from a distant location) and coalescence (the chance that  
108 they share a parent). A key early observation by Wright (1946) is that this balance is often nicely  
109 summarized by the “neighborhood size”, defined in two dimensions to be  $N_W = 4\pi\rho\sigma^2$ , where  $\sigma^2$  is  
110 one half of the mean squared parent–offspring distance and  $\rho$  is population density (see Rousset (1997)  
111 for further discussion of parameter definitions in one- and two-dimensional habitats). This can be  
112 thought of as proportional to the average number of potential mates for an individual (those within  
113 distance  $2\sigma$ ), or the number of potential parents of a randomly chosen individual. Empirical estimates  
114 of neighborhood size vary hugely across species – even in human populations, estimates range from  
115 40 to over 5,000 depending on the population and method of estimation (Table 1).

116 The first approach to modeling continuously distributed populations was to endow individuals in a  
117 Wright-Fisher model with locations in continuous space. However, since the total size of the population  
118 is constrained, this introduces interactions between arbitrarily distant individuals, which (aside from  
119 being implausible) was shown by Felsenstein (1975) to eventually lead to unrealistic population  
120 clumping if the range is sufficiently large. Another method for modeling spatial populations is to  
121 assume the existence of a grid of discrete randomly mating populations connected by migration, thus  
122 enforcing regular population density by edict. Among many other results drawn from this class of  
123 “lattice” or “stepping stone” models (Epperson 2003), Rousset (1997) showed that the slope of the linear  
124 regression of genetic differentiation ( $F_{ST}$ ) against the logarithm of spatial distance is an estimate of  
125 neighborhood size. Although these grid models may be good approximations of continuous geography  
126 in many situations, they do not model demographic fluctuations, and limit investigation of spatial  
127 structure below the level of the deme, assumptions whose impacts are unknown. An alternative  
128 method for dealing with continuous geography is a new class of coalescent models, the Spatial Lambda  
129 Fleming-Viot models (Barton *et al.* 2010; Kelleher *et al.* 2014).

130 To avoid hard-to-evaluate approximations, we here used forward-time, individual-based simulations  
131 across continuous geographical space. The question of what regulates real populations has a  
132 long history and many answers (e.g., Lloyd 1967; Antonovics and Levin 1980; Crawley 1990), but it is  
133 clear that populations must at some point have density-dependent feedback on population size, or  
134 else they would face eventual extinction or explosion. In the absence of unrealistic global population  
135 regulation, this regulation must be local, and there are many ways to achieve this (Bolker *et al.* 2003). In  
136 our simulations, each individual’s probability of survival is a decreasing function of local population  
137 density, which shifts reproductive output towards low-density regions, and produces total census sizes  
138 that fluctuate around an equilibrium. This also prevents the population clumping seen by Felsenstein  
139 (1975) (Supplemental Figure S1)). Such models have been used extensively in ecological modeling  
140 (Durrett and Levin 1994; Bolker and Pacala 1997; Law *et al.* 2003; Fournier and Méléard 2004; Champer  
141 *et al.* 2019) but rarely in population genetics, where to our knowledge implementations of continuous  
142 space models before their availability through SLiM (Haller and Messer 2019) have focused on a small

143 number of genetic loci (e.g., Slatkin and Barton 1989; Barton *et al.* 2002; Robledo-Arnuncio and Rousset  
 144 2010; Rossine 2014; Jackson and Fahrig 2014), which limits the ability to investigate the impacts of  
 145 continuous space on genome-wide genetic variation as is now routinely sampled from real organisms.  
 146 By simulating chromosome-scale sequence alignments and complete population histories we are able  
 147 to treat our simulations as real populations and replicate the sampling designs and analyses commonly  
 148 conducted on real genomic data.

#### 149 **A Forward-Time Model of Evolution in Continuous Space**

150 We simulated populations using the program SLiM v3.1 (Haller and Messer 2019). Each time step  
 151 consists of three stages: reproduction, dispersal, and mortality. To reduce the number of parameters  
 152 we use the same parameter, denoted  $\sigma$ , to modulate the spatial scale of interactions at all three stages  
 153 by adjusting the standard deviation of the corresponding Gaussian functions. Informally, we think of  
 154  $\sigma$  as the “dispersal distance”, although only one of those stages is dispersal.

155 At the beginning of the simulation individuals are distributed uniformly at random on a continuous,  
 156 square landscape. Individuals are hermaphroditic, and each time step, each produces a Poisson number  
 157 of offspring with mean  $1/L$ . Offspring disperse a Gaussian-distributed distance away from the parent  
 158 with mean zero and standard deviation  $\sigma$  in both the  $x$  and  $y$  coordinates. Each offspring is produced  
 159 with a mate selected randomly from those within distance  $3\sigma$ , with probability of choosing a neighbor  
 160 at distance  $d$  proportional to the Gaussian density with mean zero and standard deviation  $\sigma$ , which is  
 161  $g(d) = \exp(-d^2/2\sigma^2)/(2\sigma^2)$ .

162 To maintain a stable population, mortality increases with local population density. To do this we  
 163 say that individuals at distance  $d$  have a competitive interaction with strength  $g(d)$ . Then, the sum  
 164 of all competitive interactions with individual  $i$  is  $n_i = \sum_j g(d_{ij})$ , where  $d_{ij}$  is the distance between  
 165 individuals  $i$  and  $j$  and the sum is over all neighbors within distance  $3\sigma$ . Since  $g$  is a probability density,  
 166  $n_i$  is an estimate of the number of nearby individuals per unit area. Then, given a per-unit carrying  
 167 capacity  $K$ , the probability of survival until the next time step for individual  $i$  is

$$p_i = \min \left( 0.95, \frac{1}{1 + n_i/(K(1 + L))} \right). \quad (1)$$

168 We chose this functional form so that the equilibrium population density per unit area is close to  $K$ ,  
 169 and the mean lifetime is around  $L$ ; for more description see the Appendix.

170 An important step in creating any spatial model is dealing with range edges. Because local popula-  
 171 tion density is used to model competition, edge or corner populations can be assigned artificially high  
 172 fitness values because they lack neighbors within their interaction radius but outside the bounds of the  
 173 simulation. We approximate a decline in habitat suitability near edges by decreasing the probability  
 174 of survival proportional to the square root of distance to edges in units of  $\sigma$ . The final probability of  
 175 survival for individual  $i$  is then

$$s_i = p_i \min(1, \sqrt{x_i/\sigma}) \min(1, \sqrt{y_i/\sigma}) \min(1, \sqrt{(W - x_i)/\sigma}) \min(1, \sqrt{(W - y_i)/\sigma}) \quad (2)$$

176 where  $x_i$  and  $y_i$  are the spatial coordinates of individual  $i$ , and  $W$  is the width (and height) of the  
 177 square habitat. This buffer roughly counteracts the increase in fitness individuals close to the edge  
 178 would otherwise have, though the effect is relatively subtle (Figure S2).

179 To isolate spatial effects from other components of the model such as overlapping generations,  
 180 increased variance in reproductive success, and density-dependent fitness, we also implemented  
 181 simulations identical to those above except that mates are selected uniformly at random from the  
 182 population, and offspring disperse to a uniform random location on the landscape. We refer to this  
 183 model as the “random mating” model, in contrast to the first, “spatial” model.

184 We stored the full genealogy and recombination history of final-generation individuals as tree  
 185 sequences (Kelleher *et al.* 2018), as implemented in SLiM (Haller *et al.* 2019). Scripts for figures and  
 186 analyses are available at <https://github.com/kern-lab/spaceness>.

187 We ran 400 simulations for the spatial and random-mating models on a square landscape of width

188  $W = 50$  with per-unit carrying capacity  $K = 5$  (census  $N \approx 10,000$ ), average lifetime  $L = 4$ , genome  
189 size  $10^8$  bp, recombination rate  $10^{-9}$  per bp per generation, and drawing  $\sigma$  values from a uniform  
190 distribution between 0.2 and 4. To speed up the simulations and limit memory overhead we used a  
191 mutation rate of 0 in SLiM and later applied mutations to the tree sequence with msprime's `mutate`  
192 function (Kelleher *et al.* 2016). Because msprime applies mutations proportionally to elapsed time,  
193 we divided the mutation rate of  $10^{-8}$  mutations per site per generation by the average generation  
194 time estimated for each value of  $\sigma$  (see 'Demographic Parameters' below) to convert the rate to units  
195 of mutations per site per unit time. We verify that this procedure produces the same site frequency  
196 spectrum as applying mutations directly in SLiM in Figure S3, in agreement with theory (Ralph *et al.*  
197 2019b). Simulations were run for 1.6 million timesteps (approximately  $30N$  generations).

198 We also compared our model's output to a commonly-used approximation of continuous space,  
199 the stepping-stone model, which we simulated with msprime (Kelleher *et al.* 2016). These results are  
200 discussed in detail in the Appendix, but in general we find that the demographic structure of a stepping-  
201 stone model can depend strongly on the chosen discretization, and some artifacts of discretization seem  
202 to become stronger in the limit of a fine grid. For many summary statistics, finer discretizations (we  
203 used a  $50 \times 50$  grid) produced similar results to the continuous model, but this was not true for others  
204 (e.g.,  $F_{IS}$  and Tajima's  $D$ ), which differed from the continuous model *more* at finer discretizations.

## 205 **Demographic Parameters**

206 Our demographic model includes parameters that control population density ( $K$ ), mean life span ( $L$ ),  
207 and dispersal distance ( $\sigma$ ). However, nonlinearity of local demographic stochasticity causes actual  
208 realized averages of these demographic quantities to deviate from the specified values in a way that  
209 depends on the neighborhood size. Therefore, to properly compare to theoretical expectations, we  
210 empirically calculated these demographic quantities in simulations. We recorded the census population  
211 size in all simulations, and used mean population density ( $\rho$ , census size divided by total area) to  
212 compute neighborhood size as  $N_W = 4\pi\rho\sigma^2$ . To estimate generation times, we stored ages of the  
213 parents of every new individual born across 200 timesteps, after a 100 generation burn-in, and took the  
214 mean. To estimate variance in offspring number, we tracked the lifetime total number of offspring for  
215 all individuals for 100 timesteps following a 100-timestep burn-in period, and calculated the variance  
216 in number of offspring across all individuals in timesteps 50-100. All calculations were performed with  
217 information recorded in the tree sequence, using pslim (Ralph *et al.* 2019a).

218 Note that  $\sigma$  controls the dispersal of offspring away from only *one* parent (e.g., the seed parent for  
219 plants), while population genetics usually defines "dispersal distance" to be the distance to a randomly  
220 chosen one of the two parents (thus taking into account the distance from pollen parent as well).  
221 This second component – the distance between mates – has in our simulations a distribution that  
222 is of order  $\sigma$  but that depends on the population's patchiness. If both between-mate distance and  
223 dispersal distance has variance  $\sigma^2$  along each axis, then the mean squared distance to a randomly  
224 chosen parent along that axis would be  $(\sigma^2 + 2\sigma^2)/2 = 3\sigma^2/2$ . To match theory, neighborhood size  
225 should be defined in terms of *effective* dispersal distance, i.e., the mean squared displacement along an  
226 axis between parent-child pairs found moving back along a lineage (Barton *et al.* 2002), and *effective*  
227 population density (Rousset 1997). However, we use  $\sigma$  and  $\rho$  as defined here to compute  $N_W$  because  
228 these quantities are more easily observable in practice than their "effective" versions.

## 229 **Sampling**

230 Our model records the genealogy and sequence variation of the complete population, but in real data,  
231 genotypes are only observed from a relatively small number of sampled individuals. We modeled three  
232 sampling strategies similar to common data collection methods in empirical genetic studies (Figure 1).  
233 "Random" sampling selects individuals at random from across the full landscape, "point" sampling  
234 selects individuals proportional to their distance from four equally spaced points on the landscape,  
235 and "midpoint" sampling selects individuals in proportion to their distance from the middle of the  
236 landscape. Downstream analyses were repeated across all sampling strategies.

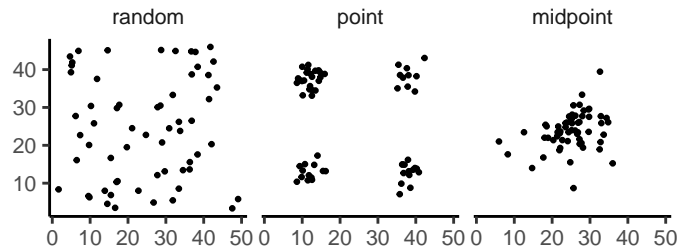


**Figure 1** Example sampling maps for 60 individuals on a  $50 \times 50$  landscape for midpoint, point, and random sampling strategies, respectively.

### 237 **Summary Statistics**

238 We calculated the site frequency spectrum and a set of 18 summary statistics (Table S1) from 60 diploid  
 239 individuals sampled from the final generation of each simulation using the python package scikit-  
 240 allel (Miles and Harding 2017). Statistics included common single-population summaries including  
 241 mean pairwise divergence ( $\pi$ ), inbreeding coefficient ( $F_{IS}$ ), and Tajima's  $D$ , as well as (motivated by  
 242 Rousset (1997)'s results) the correlation coefficient between the logarithm of the spatial distance and  
 243 the proportion of identical base pairs across pairs of individuals.

244 Following recent studies that showed strong signals for dispersal and demography in the distri-  
 245 bution of shared haplotype block lengths (e.g., Ringbauer *et al.* 2017; Baharian *et al.* 2016), we also  
 246 calculated various summaries of the distribution of pairwise identical-by-state (IBS) block lengths  
 247 among sampled chromosomes, defined to be the set of distances between adjacent sites that differ  
 248 between the two chromosomes. The full distribution of lengths of IBS tracts for each pair of chromo-  
 249 somes was first calculated with a custom python function. We then calculated the first three moments  
 250 of this distribution (mean, variance, and skew) and the number of blocks over  $10^6$  base pairs both  
 251 for each pair of individuals and for the full distribution across all pairwise comparisons. We then  
 252 calculated correlation coefficients between spatial distance and each moment of the pairwise IBS tract  
 253 distribution. Because more closely related individuals on average share longer haplotype blocks we  
 254 expect that spatial distance will be negatively correlated with mean haplotype block length, and that  
 255 this correlation will be strongest (i.e., most negative) when dispersal is low. The variance, skew, and  
 256 count of long haplotype block statistics are meant to reflect the relative length of the right (upper) tail  
 257 of the distribution, which represents the frequency of long haplotype blocks, and so should reflect  
 258 recent demographic events (Chapman and Thompson 2002). For a subset of simulations, we also  
 259 calculated cumulative distributions for IBS tract lengths across pairs of distant (more than 40 map  
 260 units) and nearby (less than 10 map units) individuals. Last, we examined the relationship between  
 261 allele frequency and the spatial dispersion of an allele by calculating the average distance between  
 262 individuals carrying each derived allele.

263 The effects of sampling on summary statistic estimates were summarized by testing for differences  
 264 in mean (ANOVA, R Core Team (2018)) and variance (Levene's test, Fox and Weisberg (2011)) across  
 265 sampling strategies for each summary statistic.

### 266 **Demographic Inference**

267 To assess the impacts of continuous spatial structure on demographic inference we inferred population  
 268 size histories for all simulations using two approaches: stairwayplot (Liu and Fu 2015) and SMC++  
 269 (Terhorst *et al.* 2016). Stairwayplot fits its model to a genome-wide estimate of the SFS, while SMC++  
 270 also incorporates linkage information. For both methods we sampled 20 individuals from all spatial  
 271 simulations using random, midpoint, and point sampling strategies.

272 As recommended by its documentation, we used stairwayplot to fit models with multiple bootstrap  
 273 replicates drawn from empirical genomic data, and took the median inferred  $N_e$  per unit time as  
 274 the best estimate. We calculated site frequency spectra with scikit-allel (Miles and Harding 2017),

generated 100 bootstrap replicates per simulation by resampling over sites, and fit models for all bootstrap samples using default settings.

For SMC++, we first output genotypes as VCF with msprime and then used SMC++'s standard pipeline for preparing input files assuming no polarization error in the SFS. We used the first individual in the VCF as the "designated individual" when fitting models, and allowed the program to estimate the recombination rate during optimization. We fit models using the 'estimate' command rather than the now recommended cross-validation approach because our simulations had only a single contig.

To evaluate the performance of these methods we binned simulations by neighborhood size, took a rolling median of inferred  $N_e$  trajectories across all model fits in a bin for each method and sampling strategy. We also examined how varying levels of isolation by distance impacted the variance of  $N_e$  estimates by calculating the standard deviation of  $N_e$  from each best-fit model.

### Association Studies

To assess the degree to which spatial structure confounds GWAS we simulated four types of nongenetic phenotype variation for 1000 randomly sampled individuals in each spatial SLiM simulation and conducted a linear regression GWAS with principal components as covariates in PLINK (Purcell *et al.* 2007). SNPs with a minor allele frequency less than 0.5% were excluded from this analysis. Phenotype values were set to vary by two standard deviations across the landscape in a rough approximation of the variation seen in height across Europe (Turchin *et al.* 2012; Garcia and Quintana-Domeque 2006, 2007). Conceptually our approach is similar to that taken by Mathieson and McVean (2012), though here we model fully continuous spatial variation and compare GWAS output across a range of dispersal distances.

In all simulations, the phenotype of each individual is determined by drawing from a Gaussian distribution with standard deviation 10 and a mean that may depend on spatial position. In spatially varying models, the mean phenotype differs by two standard deviations across the landscape. We then adjust the geographic pattern of mean phenotype to create four types of spatially autocorrelated environmental influences on phenotype. In the first simulation of *nonspatial* environments, the mean did not change, so that all individuals' phenotypes were drawn independently from a Gaussian distribution with mean 110 and standard deviation 10. Next, to simulate *clinal* environmental influences on phenotype, we increased the mean phenotype from 100 on the left edge of the range to 120 on the right edge (two phenotypic standard deviations). Concretely, the mean phenotype  $p$  for an individual at position  $(x, y)$  is  $p = 100 + 2x/5$ . Third, we simulated a more concentrated "*corner*" environmental effect by setting the mean phenotype to 120 for individuals with both  $x$  and  $y$  coordinates below 20 (two standard deviations above the rest of the map). Finally, in "*patchy*" simulations we selected 10 random points on the map and set the mean phenotype of all individuals within three map units of each of these points to 120.

We performed principal components analysis (PCA) using scikit-allel (Miles and Harding 2017) on the matrix of derived allele counts by individual for each simulation. SNPs were first filtered to remove strongly linked sites by calculating LD between all pairs of SNPs in a 200-SNP moving window and dropping one of each pair of sites with an  $R^2$  over 0.1. The LD-pruned allele count matrix was then centered and all sites scaled to unit variance when conducting the PCA, following recommendations in Patterson *et al.* (2006).

We ran linear-model GWAS both with and without the first 10 principal components as covariates in PLINK and summarized results across simulations by counting the number of SNPs with  $p$ -value below 0.05 after adjusting for an expected false positive rate of less than 5% (Benjamini and Yekutieli 2001). We also examined  $p$  values for systematic inflation by comparing to the values expected from a uniform distribution (because no SNPs were used when generating phenotypes, well-calibrated  $p$ -values should be uniform).

Results from all analyses were summarized and plotted with the "ggplot2" (Wickham 2016) and "cowplot" (Wilke 2019) packages in R (R Core Team 2018).

324 **Data Availability**

325 Scripts used for all analyses and figures are available at <https://github.com/kern-lab/spaceness>.

326 **Results**

327 **Demographic Parameters and Run Times**

328 Adjusting the spatial dispersal and interaction distance,  $\sigma$ , has a surprisingly large effect on de-  
329 mographic quantities that are usually fixed in Wright-Fisher models – the generation time, census  
330 population size, and variance in offspring number, shown in Figure 2. Because our simulation is  
331 parameterized on an individual level, these population parameters emerge as a property of the inter-  
332 actions among individuals rather than being directly set. Variation across runs occurs because, even  
333 though the parameters  $K$  and  $L$  that control population density and mean lifetime respectively were  
334 the same in all simulations, the strength of stochastic effects depends strongly on the spatial interaction  
335 distance  $\sigma$ . For instance, the population density near to individual  $i$  (denoted  $n_i$  above) is computed  
336 by averaging over roughly  $N_W = 4\pi K\sigma^2$  individuals, and so has standard deviation proportional to  
337  $1/\sqrt{N_W}$  – it is more variable at lower densities. (Recall that  $N_W$  is Wright’s neighborhood size.) Since  
338 the probability of survival is a nonlinear function of  $n_i$ , actual equilibrium densities and lifetimes differ  
339 from  $K$  and  $L$ . This is the reason that we included *random mating* simulations – where mate choice and  
340 offspring dispersal are both nonspatial – since this should preserve the random fluctuations in local  
341 population density while destroying any spatial genetic structure. We verified that random mating  
342 models retained no geographic signal by showing that summary statistics did not differ significantly  
343 between sampling regimes (Table S2), unlike in spatial models (discussed below).

344 There are a few additional things to note about Figure 2. First, all three quantities are non-monotone  
345 with neighborhood size. Census size largely declines as neighborhood size increases for both the spatial  
346 and random mating models. However, for spatial models this decline only begins for neighborhood  
347 size  $\geq 10$ . Spatial and random mating models are indistinguishable from one another for neighborhood  
348 sizes larger than 100. Census sizes range from around 14,000 at low  $\sigma$  in the random mating model  
349 to 10,000 for both models when neighborhood sizes approach 1,000. The scaling of census sizes in  
350 both random-mating and spatial models appears to be related to two consequences of the spatial  
351 competition function: the decline of fitness at range edges, which effectively reduces the habitable area  
352 by one  $\sigma$  around the edge of the map and so results in a smaller habitable area at high  $\sigma$  values; and  
353 variation in the equilibrium population density given varying competition radii. Furthermore, census  
354 size increases in spatial models as neighborhood size increases from 2 to 10. This may reflect an Allee  
355 effect (Allee *et al.* 1949) in which some individuals are unable to find mates when the mate selection  
356 radius is very small.

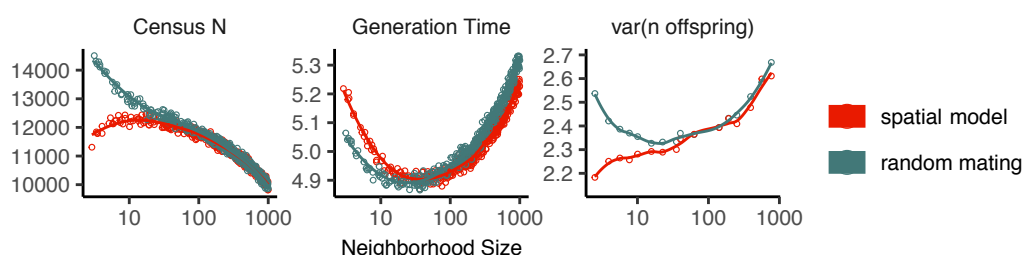
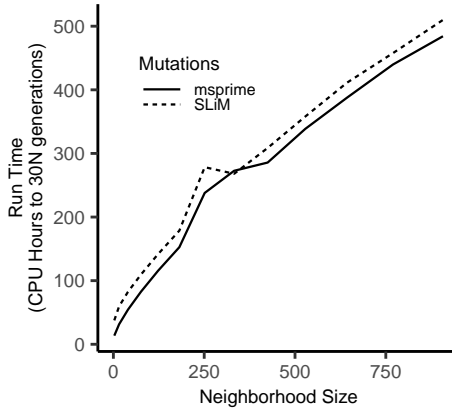


Figure 2 Genealogical parameters from spatial and random mating SLiM simulations, by neighborhood size.

357 Generation time similarly shows complex behavior with respect to neighborhood sizes, and varies  
358 between 5.2 and 4.9 timesteps per generation across the parameter range explored. Under both the  
359 spatial and random mating models, generation time reaches a minimum at a neighborhood size of  
360 around 50. Interestingly, under the range of neighborhood sizes that we examined, generation times



**Figure 3** Run times of continuous space simulations with landscape width 50 and expected density 5 under varying neighborhood size. Times are shown for simulations run with mutations applied directly in SLiM (dashed lines) or later applied to tree sequences with msprime (solid lines). Times for simulations run with tree sequence recording disabled are shown in grey.

361 between the random mating and spatial models are never quite equivalent – presumably this would  
 362 cease to be the case at neighborhood sizes higher than we simulated here.

363 Last, we looked at the variance in number of offspring – a key parameter determining the effective  
 364 population size. Surprisingly, the spatial and random mating models behave quite differently: while  
 365 the variance in offspring number increases nearly monotonically under the spatial model, the random  
 366 mating model actually shows a decline in the variance in offspring number until a neighborhood size  
 367 of around 10 before it increases and eventually equals what we observe in the spatial case.

368 Run times for our model scale approximately linearly with neighborhood size (Figure 3), with the  
 369 lowest neighborhood sizes reaching 30N generations in around a day and those with neighborhood size  
 370 approaching 1,000 requiring up to three weeks of computation. As currently implemented, running  
 371 simulations at neighborhood sizes more than 1,000 to coalescence is likely impractical, though running  
 372 these models for more limited timescales and then “recapitulating” the simulation using reverse-time  
 373 simulation from the resulting tree sequence in msprime is possible (Haller *et al.* 2019).

#### 374 **Impacts of Continuous Space on Population Genetic Summary Statistics**

375 Even though certain aspects of population demography depend on the scale of spatial interactions, it  
 376 still could be that population genetic variation is well-described by a well-mixed population model.  
 377 Indeed, mathematical results suggest that genetic variation in some spatial models should be well-  
 378 approximated by a Wright-Fisher population if neighborhood size is large and all samples are geo-  
 379 graphically widely separated (Wilkins 2004; Zähle *et al.* 2005). However, the behavior of most common  
 380 population genetic summary statistics other than Tajima’s  $D$  (Städler *et al.* 2009) has not yet been  
 381 described in realistic geographic models. Moreover, as we will show, spatial sampling strategies can  
 382 affect summaries of genetic variation at least as strongly as the underlying population dynamics.

383 **Site Frequency Spectra and Summaries of Diversity** Figure 4 shows the effect of varying neighbor-  
 384 hood size and sampling strategy on the site frequency spectrum (Figure 4, Figure S5) and several  
 385 standard population genetic summary statistics (Figure 4B; additional statistics are shown in Figure  
 386 S4). Consistent with findings in island and stepping stone simulations (Städler *et al.* 2009), the SFS  
 387 shows a significant enrichment of intermediate frequency variants in comparison to the nonspatial  
 388 expectation. This bias is most pronounced below a neighborhood size of 100 and is exacerbated by  
 389 midpoint and point sampling of individuals (depicted in Figure 1). Reflecting this, Tajima’s  $D$  is quite  
 390 positive in the same situations (Figure 4B). Notably, the point at which Tajima’s  $D$  approaches 0 differs  
 391 strongly across sampling strategies – varying from a neighborhood size of roughly 50 for random



**Figure 4** Site frequency spectrum (A; note axes are log-scaled) and summary statistic distributions (B) by sampling strategy and neighborhood size.

392 sampling to at least 1000 for midpoint sampling.

393 One of the most commonly used summaries of variation is Tajima's summary of nucleotide diversity,  
394  $\theta_\pi$ , calculated as the mean density of nucleotide differences averaged across pairs of samples. As can  
395 be seen in Figure 4B,  $\theta_\pi$  in the spatial model is inflated by up to three-fold relative to the random  
396 mating model. This pattern is opposite the expectation from census population size (Figure 2), because  
397 the spatial model has *lower* census size than the random mating model at neighborhood sizes less than  
398 100. Differences between these models likely occur because  $\theta_\pi$  is a measure of mean time to most recent  
399 common ancestor between two samples, and at small values of  $\sigma$ , the time for dispersal to mix ancestry  
400 across the range exceeds the mean coalescent time under random mating. (For instance, at the smallest  
401 value of  $\sigma = 0.2$ , the range is 250 dispersal distances wide, and since the location of a diffusively  
402 moving lineage after  $k$  generations has variance  $k\sigma^2$ , it takes around  $250^2 = 62500$  generations to  
403 mix across the range, which is roughly ten times larger than the random mating effective population  
404 size).  $\theta_\pi$  using each sampling strategy approaches the random mating expectation at its own rate, but  
405 by a neighborhood size of around 100 all models are roughly equivalent. Interestingly, the effect of  
406 sampling strategy is reversed relative to that observed in Tajima's D – midpoint sampling reaches  
407 random mating expectations around neighborhood size 50, while random sampling is inflated until  
408 around neighborhood size 100.

409 Values of observed heterozygosity and its derivative  $F_{IS}$  also depend heavily on neighborhood size  
410 under spatial models as well as the sampling scheme.  $F_{IS}$  is inflated above the expectation across  
411 most of the parameter space examined and across all sampling strategies. This effect is caused by  
412 a deficit of heterozygous individuals in low-dispersal simulations – a continuous-space version of  
413 the Wahlund effect (Wahlund 1928). Indeed, for random sampling under the spatial model,  $F_{IS}$  does  
414 not approach the random mating equivalent until neighborhood sizes of nearly 1000. On the other  
415 hand, the dependency of raw observed heterozygosity on neighborhood size is not monotone. Under  
416 midpoint sampling observed heterozygosity is inflated even over the random mating expectation, as a  
417 result of the a higher proportion of heterozygotes occurring in the middle of the landscape (Figure S6).  
418 This echoes a report from Shirk and Cushman (2014) who observed a similar excess of heterozygosity  
419 in the middle of the landscape when simulating under a lattice model.

420 **IBS tracts and correlations with geographic distance** We next turn our attention to the effect of  
421 geographic distance on haplotype block length sharing, summarized for sets of nearby and distant  
422 individuals in Figure 5. There are two main patterns to note. First, nearby individuals share more  
423 long IBS tracts than distant individuals (as expected because they are on average more closely related).  
424 Second, the difference in the number of long IBS tracts between nearby and distant individuals  
425 decreases as neighborhood size increases. This reflects the faster spatial mixing of populations with  
426 higher dispersal, which breaks down the correlation between the IBS tract length distribution and  
427 geographic distance. This can also be seen in the bottom row of Figure 4B, where the correlation  
428 coefficients between the summaries of the IBS tract length distribution (the mean, skew, and count of  
429 tracts over  $10^6$ bp) and geographic distance approaches 0 as neighborhood size increases.

430 The patterns observed for correlations of IBS tract lengths with geographic distance are similar  
431 to those observed in the more familiar correlation of allele frequency measures such as  $D_{xy}$  (i.e.,  
432 "genetic distance") or  $F_{ST}$  against geographic distance (Rousset 1997).  $D_{xy}$  is positively correlated  
433 with the geographic distance between the individuals, and the strength of this correlation declines  
434 as dispersal increases (Figure 4B), as expected (Wright 1943; Rousset 1997). This relationship is very  
435 similar across random and point sampling strategies, but is weaker for midpoint sampling, perhaps  
436 due to a dearth of long-distance comparisons. In much of empirical population genetics a regression  
437 of genetic differentiation against spatial distance is a de-facto metric of the significance of isolation  
438 by distance. The similar behavior of moments of the pairwise distribution of IBS tract lengths shows  
439 why haplotype block sharing has recently emerged as a promising source of information on spatial  
440 demography through methods described in Ringbauer *et al.* (2017) and Baharian *et al.* (2016).

441 **Spatial distribution of allele copies** Mutations occur in individuals and spread geographically over  
442 time. Because low frequency alleles generally represent recent mutations (Sawyer 1977; Griffiths *et al.*

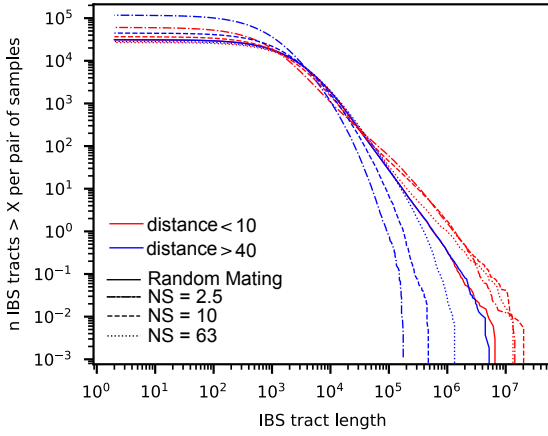


**Figure 5** Cumulative distributions for IBS tract lengths per pair of individuals at different geographic distances, across three neighborhood sizes (NS). Nearby pairs (red curves) share many more long IBS tracts than do distant pairs (blue curves), except in the random mating model. The distribution of long IBS tracts between nearby individuals are very similar across neighborhood sizes, but distant individuals are much more likely to share long IBS tracts at high neighborhood size than at low neighborhood size.

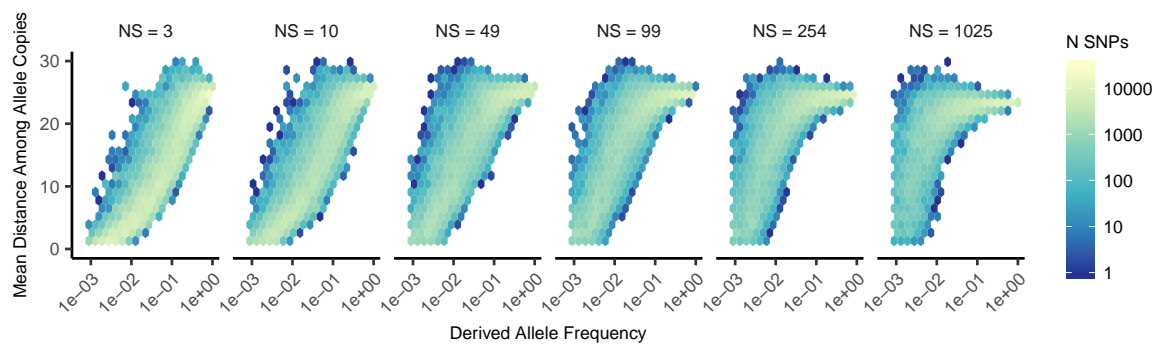


**Figure 6** Spatial spread of rare alleles by neighborhood size (NS): Each plot shows the distribution (across derived alleles and simulations) of average pairwise distance between individuals carrying a focal derived allele and derived allele frequency.

443 1999), the geographic spread of an allele may covary along with its frequency in the population. To  
444 visualize this relationship we calculated the average distance among individuals carrying a focal  
445 derived allele across simulations with varying neighborhood sizes, shown in Figure 6. On average  
446 we find that low frequency alleles are the most geographically restricted, and that the extent to which  
447 geography and allele frequency are related depends on the amount of dispersal in the population.  
448 For populations with large neighborhood sizes we found that even very low frequency alleles can be  
449 found across the full landscape, whereas in populations with low neighborhood sizes the relationship  
450 between distance among allele copies and their frequency is quite strong. This is the basic process  
451 underlying Nembret and Slatkin's (2009) method for estimating dispersal distances based on the  
452 distribution of low frequency alleles, and also generates the greater degree of bias in GWAS effect sizes  
453 for low frequency alleles identified in Mathieson and McVean (2012).

#### 454 **Effects of Space on Demographic Inference**

455 One of the most important uses for population genetic data is inferring demographic history of popu-  
456 lations. As demonstrated above, the site frequency spectrum and the distribution of IBS tracts varies  
457 across neighborhood sizes and sampling strategies. Does this variation lead to different inferences of  
458 past population sizes? To ask this we inferred population size histories from samples drawn from our  
459 simulated populations with two approaches: stairwayplot (Liu and Fu 2015), which uses a genome-  
460 wide estimate of the SFS, and SMC++ (Terhorst *et al.* 2016), which incorporates information on both the  
461 SFS and linkage disequilibrium across the genome.

462 Figure 7A shows rolling medians of inferred population size histories from each method across all  
463 simulations, grouped by neighborhood size and sampling strategy. In general these methods tend to  
464 slightly overestimate ancient population sizes and infer recent population declines when neighborhood  
465 sizes are below 20 and sampling is spatially clustered. The overestimation of ancient population sizes  
466 however is relatively minor, averaging around a two-fold inflation at 10,000 generations before present  
467 in the worst-affected bins. For stairwayplot we found that many runs infer dramatic population  
468 bottlenecks in the last 1,000 generations when sampling is spatially concentrated, resulting in ten-fold  
469 or greater underestimates of recent population sizes. However SMC++ appeared more robust to  
470 this error, with runs on point- and midpoint-sampled simulations at the lowest neighborhood sizes  
471 underestimating recent population sizes by roughly half and those on randomly sampled simulations  
472 showing little error. Above neighborhood sizes of around 100, both methods performed relatively well  
473 when averaging across results from multiple simulations.

474 However, individual simulations were often inferred to have turbulent demographic histories, as  
475 shown by the individually inferred histories (shown in Figure S7). Indeed, the standard deviation of  
476 inferred  $N_e$  across time points (shown in Figure 7B) often exceeds the expected  $N_e$  for both methods.  
477 That is, despite the nearly constant population sizes in our simulations, both methods tended to infer  
478 large fluctuations in population size over time, which could potentially result in incorrect biological  
479 interpretations. On average the variance of inferred population sizes was elevated at the lowest  
480 neighborhood sizes and declines as dispersal increases, with the strongest effects seen in stairwayplot  
481 results with clustered sampling and neighborhood sizes less than 20 (Figure 7B).

#### 482 **GWAS**

483 To ask what confounding effects spatial genetic variation might have on genome-wide association  
484 studies we performed GWAS on our simulations using phenotypes that were determined solely by  
485 the environment – so, any SNP showing statistically significant correlation with phenotype is a false  
486 positive. As expected, spatial autocorrelation in the environment causes spurious associations across  
487 much of the genome if no correction for genetic relatedness among samples is performed (Figures 8 and  
488 S8). This effect is particularly strong for clinal and corner environments, for which the lowest dispersal  
489 levels cause over 60% of SNPs in the sample to return significant associations. Patchy environmental  
490 distributions, which are less strongly spatially correlated (Figure 8A), cause fewer false positives  
491 overall but still produce spurious associations at roughly 10% of sites at the lowest neighborhood  
492 sizes. Interestingly we also observed a small number of false positives in roughly 3% of analyses

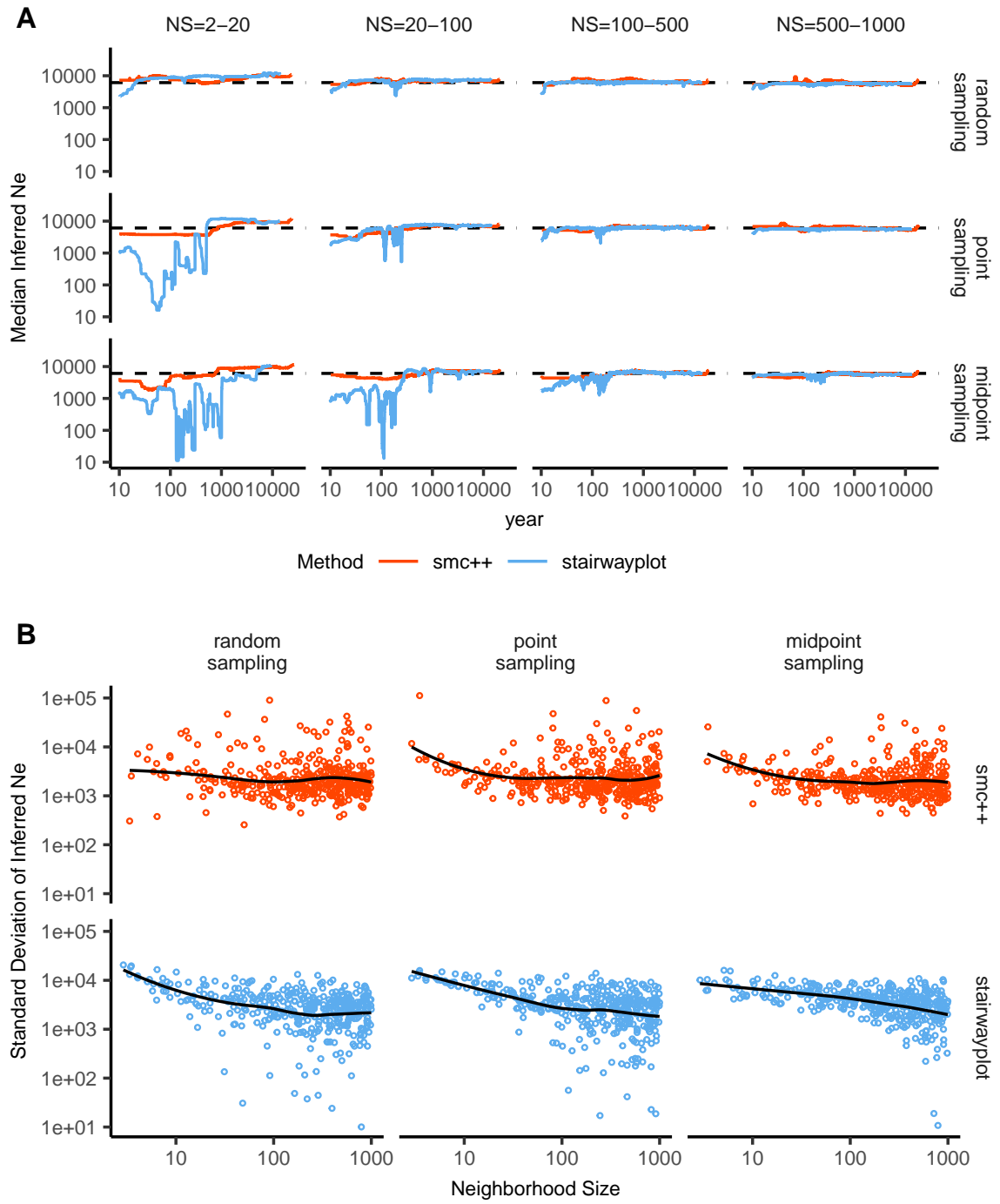


**Figure 7** A: Rolling median inferred  $N_e$  trajectories for stairwayplot and smc++ across sampling strategies and neighborhood size bins. The dotted line shows the mean  $N_e$  of random-mating simulations. B: Standard deviation of individual inferred  $N_e$  trajectories, by neighborhood size and sampling strategy. Black lines are loess curves. Plots including individual model fits are shown in Figure S7.

493 on simulations with nonspatial environments, both with and without PC covariates included in the  
494 regression.

495 The confounding effects of geographic structure are well known, and it is common practice to  
496 control for this by including principal components (PCs) as covariates to control for these effects. This  
497 mostly works in our simulations – after incorporating the first ten PC axes as covariates, the vast  
498 majority of SNPs no longer surpass a significance threshold chosen to have a 5% false discovery rate  
499 (FDR). However, a substantial number of SNPs – up to 1.5% at the lowest dispersal distances – still  
500 surpass this threshold (and thus would be false positives in a GWAS), especially under “corner” and  
501 “patchy” environmental distributions (Figure 8C). At neighborhood sizes larger than 500, up to 0.31%  
502 of SNPs were significant for corner and clinal environments. Given an average of 132,000 SNPs across  
503 simulations after MAF filtering, this translates to up to 382 false-positive associations; for human-sized  
504 genomes, this number would be much larger. In most cases the  $p$  values for these associations were  
505 significant after FDR correction but would not pass the threshold for significance under the more  
506 conservative Bonferroni correction (see example Manhattan plots in figure S8).

507 Clinal environments cause an interesting pattern in false positives after PC correction: at low  
508 neighborhood sizes the correction removes nearly all significant associations, but at neighborhood  
509 sizes above roughly 250 the proportion of significant SNPs increases to up to 0.4% (Figure 8). This may  
510 be due to a loss of descriptive power of the PCs – as neighborhood size increases, the total proportion of  
511 variance explained by the first 10 PC axes declines from roughly 10% to 4% (Figure 8B). Essentially, PCA  
512 seems unable to effectively summarize the weak population structure present in large-neighborhood  
513 simulations given the sample sizes we tested, but these populations continue to have enough spatial  
514 structure to create significant correlations between genotypes and the environment. A similar process  
515 can also be seen in the corner phenotype distribution, in which the count of significant SNPs initially  
516 declines as neighborhood size increases and then increases at approximately the point at which the  
517 proportion of variance explained by PCA approaches its minimum.

518 Figure 8D shows quantile-quantile plots for a subset of simulations that show the degree of genome-  
519 wide inflation of test statistics in PC-corrected GWAS across all simulations and environmental distri-  
520 butions. An alternate visualization is also included in figure S9. For clinal environments,  $-\log_{10}(p)$   
521 values are most inflated when neighborhood sizes are large, consistent with the pattern observed in  
522 the count of significant associations after PC regression. In contrast corner and patchy environments  
523 cause the greatest inflation in  $-\log_{10}(p)$  at neighborhood sizes less than 100, which likely reflects  
524 the inability of PCA to account for fine-scale structure caused by very limited dispersal. Finally, we  
525 observed that PC regression appears to overfit to some degree for all phenotype distributions, visible  
526 in Figure 8D as points falling below the 1:1 line.

## 527 Discussion

528 In this study, we have used efficient forward time population genetic simulations to describe the  
529 myriad influence of continuous geography on genetic variation. In particular, we examine how three  
530 main types of downstream empirical inference are affected by unmodeled spatial population structure  
531 – population genetic summary statistics, inference of population size history, and genome-wide associ-  
532 ation studies (GWAS). As discussed above, space often matters (and sometimes dramatically), both  
533 because of how samples are arranged in space, and because of the inherent patterns of relatedness  
534 established by geography.

### 535 Effects of Dispersal

536 Limited dispersal inflates effective population size, creates correlations between genetic and spatial  
537 distances, and introduces strong distortions in the site frequency spectrum that are reflected in a  
538 positive Tajima’s  $D$  (Figure 4). At the lowest dispersal distances, this can increase genetic diversity  
539 threefold relative to random-mating expectations. These effects are strongest when neighborhood  
540 sizes are below 100, but in combination with the effects of nonrandom sampling they can persist up to  
541 neighborhood sizes of at least 1000 (e.g., inflation in Tajima’s  $D$  and observed heterozygosity under  
542 midpoint sampling). If samples are chosen uniformly from across space, the general pattern is similar

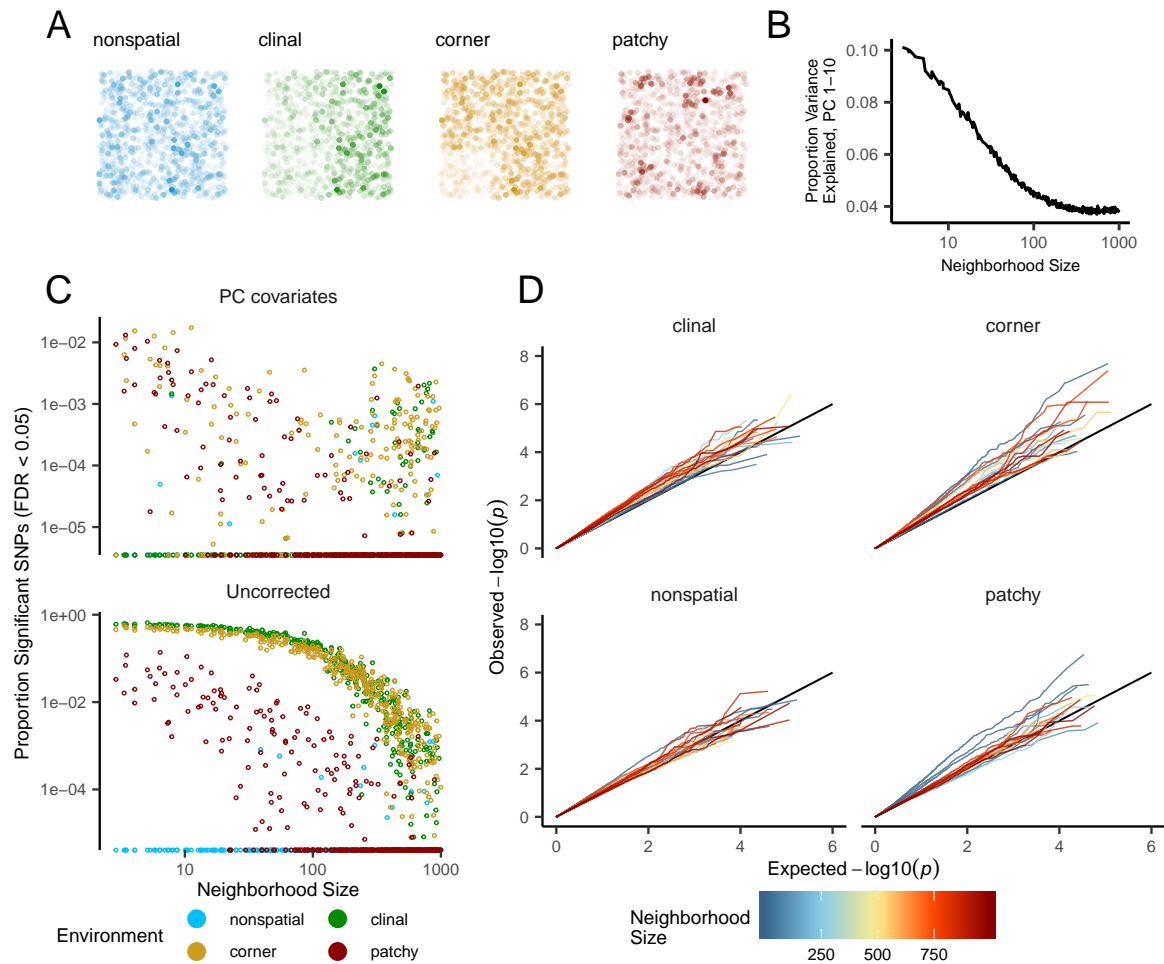


**Figure 8** Impacts of spatially varying environments and isolation by distance on linear regression GWAS. Simulated quantitative phenotypes are determined only by an individual's location and the spatial distribution of environmental factors. In **A** we show the phenotypes and locations of sampled individuals under four environmental distributions, with transparency scaled to phenotype. As neighborhood size increases a PCA explains less of the total variation in the data (**B**). Spatially correlated environmental factors cause false positives at a large proportion of SNPs, which is partially but not entirely corrected by adding the first 10 PC coordinates as covariates (**C**). Quantile-quantile plots in **(D)** show inflation of  $-\log_{10}(p)$  after PC correction for simulations with spatially structured environments, with line colors showing the neighborhood size of each simulation.

543 to expectations of the original analytic model of Wright (1943), which predicts that populations with  
544 neighborhood sizes under 100 will differ substantially from random mating, while those above 10,000  
545 will be nearly indistinguishable from panmixia.

546 The patterns observed in sequence data reflect the effects of space on the underlying genealogy.  
547 Nearby individuals coalesce rapidly under limited dispersal and so are connected by short branch  
548 lengths, while distant individuals take much longer to coalesce than they would under random  
549 mating. Mutation and recombination events in our simulation both occur at a constant rate along  
550 branches of the genealogy, so the genetic distance and number of recombination events separating  
551 sampled individuals simply gives a noisy picture of the genealogies connecting them. Tip branches  
552 (i.e., branches subtending only one individual) are then relatively short, and branches in the middle of  
553 the genealogy connecting local groups of individuals relatively long, leading to the biases in the site  
554 frequency spectrum shown in Figure 4.

555 The genealogical patterns introduced by limited dispersal are particularly apparent in the distribution  
556 of haplotype block lengths (Figure 4). This is because identical-by-state tract lengths reflect the  
557 impacts of two processes acting along the branches of the underlying genealogy – both mutation and  
558 recombination – rather than just mutation as is the case when looking at the site frequency spectrum or  
559 related summaries. This means that the pairwise distribution of haplotype block lengths carries with  
560 it important information about genealogical variation in the population, and correlation coefficients  
561 between moments of the this distribution and geographic location contain signal similar to the correlations  
562 between  $F_{ST}$  or  $D_{xy}$  and geographic distance (Rousset 1997). Indeed this basic logic underlies  
563 two recent studies explicitly estimating dispersal from the distribution of shared haplotype block  
564 lengths (Ringbauer *et al.* 2017; Baharian *et al.* 2016). Conversely, because haplotype-based measures of  
565 demography are particularly sensitive to variation in the underlying genealogy, inference approaches  
566 that assume random mating when analyzing the distribution of shared haplotype block lengths are  
567 likely to be strongly affected by spatial processes.

### 568 **Effects of Sampling**

569 One of the most important differences between random mating and spatial models is the effect of  
570 sampling: in a randomly mating population the spatial distribution of sampling effort has no effect on  
571 estimates of genetic variation (Table S1), but when dispersal is limited sampling strategy can compound  
572 spatial patterns in the underlying genealogy and create pervasive impacts on all downstream genetic  
573 analyses (see also Städler *et al.* (2009)). In most species, the difficulty of traveling through all parts  
574 of a species range and the inefficiency of collecting single individuals at each sampling site means  
575 that most studies follow something closest to the “point” sampling strategy we simulated, in which  
576 multiple individuals are sampled from nearby points on the landscape. For example, in ornithology a  
577 sample of 10 individuals per species per locality is a common target when collecting for natural history  
578 museums. In classical studies of *Drosophila* variation the situation is considerably worse, in which a  
579 single orchard might be extensively sampled.

580 When sampling is clustered at points on a landscape and dispersal is limited, the sampled individuals  
581 will be more closely related than a random set of individuals. Average coalescence times of  
582 individuals collected at a locality will then be more recent and branch lengths shorter than expected by  
583 analyses assuming random mating. This leads to fewer mutations and recombination events occurring  
584 since their last common ancestor, causing a random set of individuals to share longer average IBS tracts  
585 and have fewer nucleotide differences. For some data summaries, such as Tajima’s  $D$ , Watterson’s  
586  $\theta$ , or the correlation coefficient between spatial distance and the count of long haplotype blocks, this  
587 can result in large differences in estimates between random and point sampling (Figure 4). Inferring  
588 underlying demographic parameters from these summary statistics – unless the spatial locations of the  
589 sampled individuals are somehow taken into account – will likely be subject to bias.

590 We observed the largest sampling effects using “midpoint” sampling. This model is meant to  
591 reflect a bias in sampling effort towards the middle of a species’ range. In empirical studies this  
592 sampling strategy could arise if, for example, researchers choose to sample the center of the range  
593 and avoid range edges to maximize probability of locating individuals during a short field season.  
594 Because midpoint sampling provides limited spatial resolution it dramatically reduces the magnitude

595 of observed correlations between spatial and genetic distances. More surprisingly, midpoint sampling  
596 also leads to strongly positive Tajima's  $D$  and an inflation in the proportion of heterozygous individuals  
597 in the sample – similar to the effect of sampling a single deme in an island model as reported in Städler  
598 *et al.* (2009). This increase in observed heterozygosity appears to reflect the effects of range edges,  
599 which are a fundamental facet of spatial genetic variation. If individuals move randomly in a finite  
600 two-dimensional landscape then regions in the middle of the landscape receive migrants from all  
601 directions while those on the edge receive no migrants from at least one direction. The average number  
602 of new mutations moving into the middle of the landscape is then higher than the number moving  
603 into regions near the range edge, leading to higher heterozygosity and lower inbreeding coefficients  
604 ( $F_{IS}$ ) away from range edges. Though here we used only a single parameterization of fitness decline at  
605 range edges we believe this is a general property of non-infinite landscapes as it has also been observed  
606 in previous studies simulating under lattice models (Neel *et al.* 2013; Shirk and Cushman 2014).

607 In summary, we recommend that empirical researchers collect individuals from across as much  
608 of the species' range as practical, choosing samples separated by a range of spatial scales. Many  
609 summary statistics are designed for well-mixed populations, and so provide different insights into  
610 genetic variation when applied to different subsets of the population. Applied to a cluster of samples,  
611 summary statistics based on segregating sites (e.g., Watterson's  $\theta$  and Tajima's  $D$ ), heterozygosity, or  
612 the distribution of long haplotype blocks, can be expected to depart significantly from what would be  
613 obtained from a wider distribution of samples. Comparing the results of analyses conducted on all  
614 individuals versus those limited to single individuals per locality can provide an informative contrast.  
615 Finally we wish to point out that the bias towards intermediate allele frequencies that we observe may  
616 mean that the importance of linked selection, at least as is gleaned from the site frequency spectrum,  
617 may be systematically underestimated currently.

### 618 **Demography**

619 Previous studies have found that population structure and nonrandom sampling can create spurious  
620 signals of population bottlenecks when attempting to infer demographic history with microsatellite  
621 variation, summary statistics, or runs of homozygosity (Chikhi *et al.* 2010; Städler *et al.* 2009; Ptak  
622 and Przeworski 2002; Mazet *et al.* 2015; Leblois *et al.* 2006). Here we found that methods that infer  
623 detailed population trajectories through time based on the SFS and patterns of LD across the genome  
624 are also subject to this bias, with some combinations of dispersal and sampling strategy systematically  
625 inferring deep recent population bottlenecks and overestimating ancient  $N_e$  by around a factor of 2.  
626 We were surprised to see that both stairwayplot and SMC++ can tolerate relatively strong isolation by  
627 distance – i.e., neighborhood sizes of 20 – and still perform well when averaging results across multiple  
628 simulations. (However, note the high amount of between-simulation variance seen in Figure S7.)  
629 Inference in populations with neighborhood sizes over 20 was relatively unbiased unless samples were  
630 concentrated in the middle of the range (Figure 7). Although median demography estimates across  
631 many independent simulations were fairly accurate, empirical work has only a single estimate to work  
632 with, and individual model fits (Figure S7) suggest that spuriously inferred population size changes  
633 and bottlenecks are common, especially at small neighborhood sizes. As we will discuss below, most  
634 empirical estimates of neighborhood size, including all estimates for human populations, are large  
635 enough that population size trajectories inferred by these approaches should not be strongly affected by  
636 spatial biases created by dispersal in continuous landscapes. In contrast, Mazet *et al.* (2015) found that  
637 varying migration rates through time could create strong biases in inferred population trajectories from  
638 an  $n$ -island model with parameters relevant for human history, suggesting that changes in migration  
639 rates through time are more likely to drive variation in inferred  $N_e$  than isolation by distance.

640 We found that SMC++ was more robust to the effects of space than stairwayplot, underestimating  
641 recent populations by roughly half in the worst time periods rather than nearly 10-fold as with  
642 stairwayplot. Though this degree of variation in population size is certainly meaningful in an ecological  
643 context, it is relatively minor in population genetic terms. Methods directly assessing haplotype  
644 structure in phased data example, (e.g., Browning and Browning 2015) are thought to provide increased  
645 resolution for recent demographic events, but in this case the error we observed was essentially an  
646 accurate reflection of underlying genealogies in which terminal branches are anomalously short.

647 Combined with our analysis of IBS tract length variation (Figure 5) this suggests that haplotype-based  
648 methods are likely to be affected by similar biases.

649 A more worrying pattern was the high level of variance in inferred  $N_e$  trajectories for individual  
650 model fits using these methods, which was highest in simulations with the smallest neighborhood  
651 size (Figure 7, Figure S7). This suggests that, at a minimum, researchers working with empirical data  
652 should replicate analyses multiple times and take a rolling average if model fits are inconsistent across  
653 runs. Splitting samples and running replicates on separate subsets – the closest an empirical study can  
654 come to our design of averaging the results from multiple simulations – may also alleviate this issue.

655 Our analysis suggests that many empirical analyses of population size history using methods like  
656 SMC++ are robust to error caused by spatial structure within continuous landscapes. Inferences drawn  
657 from static SFS-based methods like stairwayplot should be treated with caution when there are signs  
658 of isolation by distance in the underlying data (for example, if a regression of  $F_{ST}$  against the logarithm  
659 of geographic distance has a significantly positive slope), and in particular an inference of population  
660 bottlenecks in the last 1000 years should be discounted if sampling is clustered, but estimates of deeper  
661 time patterns are likely to be fairly accurate. The biases in the SFS and haplotype structure identified  
662 above (see also Wakeley 1999; Chikhi *et al.* 2010; Städler *et al.* 2009) are apparently small enough that  
663 they fall within the range of variability regularly inferred by these approaches, at least on datasets of  
664 the size we simulated.

## 665 **GWAS**

666 Spatial structure is particularly challenging for genome-wide association studies, because the effects of  
667 dispersal on genetic variation are compounded by spatial variation in the environment (Mathieson  
668 and McVean 2012). Spatially restricted mate choice and dispersal causes variation in allele frequencies  
669 across the range of a species. If environmental factors affecting the phenotype of interest also vary over  
670 space, then allele frequencies and environmental exposures will covary over space. In this scenario an  
671 uncorrected GWAS will infer genetic associations with a purely environmental phenotype at any site  
672 in the genome that is differentiated over space, and the relative degree of bias will be a function of the  
673 degree of covariation in allele frequencies and the environment (i.e., Figure 8C, bottom panel). This  
674 pattern has been demonstrated in a variety of simulation and empirical contexts (Price *et al.* 2006; Yu  
675 *et al.* 2005; Young *et al.* 2018; Mathieson and McVean 2012; Kang *et al.* 2008, 2010; Bulik-Sullivan *et al.*  
676 2015; Berg *et al.* 2018; Sohail *et al.* 2018).

677 Incorporating PC positions as covariates in a linear-regression GWAS (Price *et al.* 2006) is designed  
678 to address this challenge by regressing out a baseline level of “average” differentiation. In essence, a  
679 PC-corrected GWAS asks “what regions of the genome are more associated with this phenotype than  
680 the average genome-wide association observed across populations?” In our simulations, we observed  
681 that this procedure can fail under a variety of circumstances. If dispersal is limited and environmental  
682 variation is clustered in space (i.e., corner or patchy distributions in our simulations), PC positions fail  
683 to capture the fine-scale spatial structure required to remove all signals of association. Conversely, as  
684 dispersal increases, PCA loses power to describe population structure before spatial mixing breaks  
685 down the relationship between genotype and the environment. These effects were observed with all  
686 spatially correlated environmental patterns, but were particularly pronounced if environmental effects  
687 are concentrated in one region, as was also found by Mathieson and McVean (2012). Though increasing  
688 the number of PC axes used in the analysis may reduce the false-positive rate, this may also decrease  
689 the power of the test to detect truly causal alleles (Lawson *et al.* 2019).

690 In this work we simulated a single chromosome with size roughly comparable to one human  
691 chromosome. If we scale the number of false-positive associations identified in our analyses to a  
692 GWAS conducted on whole-genome data from humans, we would expect to see several thousand  
693 weak false-positive associations after PC corrections in a population with neighborhood sizes up to at  
694 least 1000 (which should include values appropriate for many human populations). Notably, very few  
695 of the spurious associations we identified would be significant at a conservative Bonferroni-adjusted  
696  $p$ -value cutoff (see Figure S8). This suggests that GWAS focused on finding strongly associated alleles  
697 for traits controlled by a limited number of variants in the genome are likely robust to the impacts of  
698 continuous spatial structure. However, methods that analyze the combined effects of thousands or

699 millions of weakly associated variants such as polygenic risk scores (Wray *et al.* 2007; International  
700 Schizophrenia Consortium *et al.* 2009) are likely to be affected by subtle population structure. Indeed  
701 as recently identified in studies of genotype associations for human height in Europe (Berg *et al.* 2018;  
702 Sohail *et al.* 2018), PC regression GWAS in modern human populations do include residual signal of  
703 population structure in large-scale analyses of polygenic traits. In addition to error associated with  
704 varying patterns of linkage disequilibrium and allele frequency among populations, the confounding  
705 of environmental and genetic effects on phenotypes introduced by population structure is expected to  
706 lead to low predictive power when polygenic scores are generated for populations outside the original  
707 GWAS cohort, as was shown in a recent study finding lower polygenic score predictive power outside  
708 European populations (Martin *et al.* 2019).

709 In summary, spatial covariation in population structure and the environment confounds the interpretation  
710 of GWAS *p*-values, and correction using principal components is insufficient to fully  
711 separate these signals for polygenic traits under a variety of environmental and population parameter  
712 regimes. Other GWAS methods such as mixed models (Kang *et al.* 2008) may be less sensitive to  
713 this confounding, but there is no obvious reason that this should be so. One approach to estimating  
714 the degree of bias in GWAS caused by population structure is LD score regression (Bulik-Sullivan  
715 *et al.* 2015). Though this approach appears to work well in practice, its interpretation is not always  
716 straightforward and it is likely biased by the presence of linked selection (Berg *et al.* 2018). In addition,  
717 we observed that in many cases the false-positive SNPs we identified appeared to be concentrated in  
718 LD peaks similar to those expected from truly causal sites (Figure S8), which may confound LD score  
719 regression.

720 We suggest a straightforward alternative for species in which the primary axes of population  
721 differentiation are associated with geography (note this is likely not the case for some modern human  
722 populations): run a GWAS with spatial coordinates as phenotypes and check for *p*-value inflation or  
723 significant associations. If significant associations with sample locality are observed after correcting for  
724 population structure, the method is sensitive to false positives induced by spatial structure. This is  
725 essentially the approach taken in our "clinal" model (though we add normally distributed noise to our  
726 phenotypes). This approach has recently been taken with polygenic scores for UK Biobank samples  
727 in Haworth *et al.* (2019), finding that scores are correlated with birth location even in this relatively  
728 homogenous sample. Of course, it is possible that genotypes indirectly affect individual locations by  
729 adjusting organismal fitness and thus habitat selection across spatially varying environments, but we  
730 believe that this hypothesis should be tested against a null of stratification bias inflation rather than  
731 accepted as true based on GWAS results.

### 732 **Where are natural populations on this spectrum?**

733 For how much of the tree of life do spatial patterns circumscribe genomic variation? In Table 1 we  
734 gathered estimates of neighborhood size from a range of organisms to get an idea of how strongly local  
735 geographic dispersal affects patterns of variation. This is an imperfect measure: some aspects of genetic  
736 variation are most strongly determined by neighborhood size (Wright 1946), others (e.g., number of  
737 segregating sites) by global  $N_e$ , or the ratio of the two. In addition, definitions of "population density"  
738 in genetic versus ecological studies may lead to varying estimates of neighborhood size for a given  
739 species, and these empirical examples may be biased towards small-neighborhood species because few  
740 studies have quantified neighborhood size in species with very high dispersal or population density.

741 However, from the available data we find that neighborhood sizes in the range we simulated are  
742 fairly common across a range of taxa. At the extreme low end of empirical neighborhood size estimates  
743 we see some flowering plants, large mammals, and colonial insects like ants with neighborhood sizes  
744 less than roughly 100. Species such as this have neighborhood size estimates small enough that spatial  
745 processes are likely to strongly influence inference. These include some human populations such as  
746 the Gainj- and Kalam-speaking people of Papua New Guinea, in which the estimated neighborhood  
747 sizes in Rousset (1997) range from 40 to 410 depending on the method of estimation. Many more  
748 species occur in a middle range of neighborhood sizes between 100 and 1000 – a range in which spatial  
749 processes play a minor role in our analyses under random spatial sampling but are important when  
750 sampling of individuals in space is clustered. Surprisingly, even some flying insects with huge census

**Table 1 Neighborhood size estimates from empirical studies.**

Species	Description	Neighborhood Size	Method	Citation
<i>Ipomopsis aggregata</i>	flowering plant	12.60 - 37.80	Genetic	(Campbell and Dooley 1992)
<i>Borrichia frutescens</i>	salt marsh plant	20 - 30	Genetic+Survey	(Antlfinger 1982)
<i>Oreamnos americanus</i>	mountain goat	36 - 100	Genetic	(Shirk and Cushman 2014)
<i>Homo sapiens</i>	Gainj- and Kalam-speaking people, Papua New Guinea	40 - 213	Genetic	(Rousset 1997)
<i>Formica sp.</i>	colonial ants	50 - 100	Genetic	(Pamilo 1983)
<i>Astrocaryum mexicanum</i>	palm tree	102 - 895	Genetic+survey	(Eguiarte <i>et al.</i> 1993)
<i>Spermophilus mollis</i>	ground squirrel	204 - 480	Genetic+Survey	(Antolin <i>et al.</i> 2001)
<i>Sceloporus olivaceus</i>	lizard	225 - 270	Survey	(Kerster 1964)
<i>Dieffenbachia longispatha</i>	beetle-pollinated colonial herb	227 - 611	Survey	(Young 1988)
<i>Aedes aegypti</i>	Yellow-fever mosquito	268	Genetic	(Jasper <i>et al.</i> 2019)
<i>Homo sapiens</i>	Gainj- and Kalam-speaking people, Papua New Guinea	410	Survey	(Rousset 1997)
<i>Quercus laevis</i>	Oak tree	> 440	Genetic	(Berg and Hamrick 1995)
<i>Drosophila pseudoobscura</i>	fruit fly	500 - 1,000	Survey+Crosses	(Wright 1946)
<i>Homo sapiens</i>	POPRES data NE Europe	1,342 - 5,425	Genetic	(Ringbauer <i>et al.</i> 2017)

751 population sizes fall in this group, including fruit flies (*D. melanogaster*) and mosquitoes (*A. aegypti*).  
752 Last, many species likely have neighborhood sizes much larger than we simulated, including the  
753 recent ancestors of modern humans in northeastern Europe (Ringbauer *et al.* 2017). For these species  
754 demographic inference and summary statistics are likely to reflect minimal bias from spatial effects as  
755 long as dispersal is truly continuous across the landscape. While that is so we caution that association  
756 studies in which the effects of population structure are confounded with spatial variation in the  
757 environment are still sensitive to dispersal even at these large neighborhood sizes.

#### 758 ***Other demographic models***

759 Any simulation of a population of reproducing organisms requires some kind of control on population  
760 sizes, or else the population will either die out or grow very large after a sufficiently long period of time.  
761 The usual choice of population regulation for population genetics – a constant size, as in the Wright–  
762 Fisher model – implies biologically unrealistic interactions between geographically distant parts of the  
763 species range. Our choice to regulate population size by including a local density-dependent control  
764 on mortality is only one of many possible ways to do this. We could have instead regulated fecundity,  
765 or recruitment, or both; this general class of models is sometimes referred to as the “Bolker–Pacala  
766 model” (Bolker and Pacala 1997). It is not currently clear how much different choices of demographic  
767 parameters, or of functional forms for the regulation, might quantitatively affect our results, although  
768 the general predictions should be robust to similar forms of regulation. As is usual in population  
769 genetics, the populations are entirely *intrinsically* regulated. Alternatively, population size could be  
770 regulated by interactions with other species (e.g., a Lotka–Volterra model), or extrinsically specified  
771 by local resource availability (e.g., by food or nest site availability). Indeed, our model could be  
772 interpreted as a caricature of such a model: as local density increases, good habitat is increasingly  
773 occupied, pushing individuals into more marginal habitat and increasing their mortality. Many such  
774 models should behave similarly to ours, but others (especially those with local population cycling),  
775 may differ dramatically.

776 Population genetic simulations often use grids of discrete demes, which are assumed to approximate  
777 continuous space. However, there are theoretical reasons to expect that increasingly fine grids of  
778 discrete demes do not approach the continuous model (Barton *et al.* 2002). If continuous space can  
779 be approximated by a limit of discrete models, this should be true regardless of the precise details  
780 of the discrete model. Although we carefully chose parameters to match our continuous models, we  
781 found that some aspects of genetic variation diverged from the continuous case as the discretization  
782 got finer. This suggests that these models do not converge in the limit. However, many populations  
783 may indeed be well-modeled as a series of discrete, randomly-mating demes if, for example, suitable  
784 habitats are patchily distributed across the landscape. There is a clear need for greater exploration of  
785 the consequences for population genetics of ecologically realistic population models.

#### 786 ***Future Directions and Limitations***

787 As we have shown, a large number of population genetic summary statistics contain information about  
788 spatial population processes. We imagine that combinations of such summaries might be sufficient  
789 for the construction of supervised machine learning regressors (e.g., Schrider and Kern 2018) for the  
790 accurate estimation of dispersal from genetic data. Indeed, Ashander *et al.* (2018) found that inverse  
791 interpolation on a vector of summary statistics provided a powerful method of estimating dispersal  
792 distances. Expanding this approach to include the haplotype-based summary statistics studied here  
793 and applying machine learning regressors built for general inference of nonlinear relationships from  
794 high-dimensional data may allow precise estimation of spatial parameters under a range of complex  
795 models.

796 One facet of spatial variation that we did not address in this study is the confounding of dispersal  
797 and population density implicit in the definition of Wright’s neighborhood size. Our simulations were  
798 run under constant densities, but Guindon *et al.* (2016) and Ringbauer *et al.* (2017) have shown that  
799 these parameters are identifiable under some continuous models. Similarly, though the scaling effects  
800 of dispersal we show in Figure 4 should occur in populations of any total size, other aspects such as  
801 the number of segregating sites are also likely affected by the total landscape size (and so total census

size). Indeed, our finding that stepping-stone and continuous-space models match in only certain aspects of genetic variation (Figure A1) shows that qualitatively similar models can produce different results dependent on the specific parameterizations used. While we believe our continuous model is a more appropriate depiction of many species' demographies than lattice models, it is likely that some populations and breeding systems do more closely resemble a series of interconnected random-mating populations. As with all population models, the best approximation for any empirical system will depend on the natural history of the species in question. Much additional work remains to be done to better understand how life history, range size, and habitat geometry interact to shape genetic variation in continuous space, which we leave to future studies.

Though our simulation allows incorporation of realistic demographic and spatial processes, it is inevitably limited by the computational burden of tracking tens or hundreds of thousands of individuals in every generation. In particular, computations required for mate selection and spatial competition scale approximately with the product of the total census size and the neighborhood size and so increase rapidly for large populations and dispersal distances. The reverse-time spatial Lambda–Fleming–Viot model described by Barton *et al.* (2010) and implemented by Kelleher *et al.* (2014) allows exploration of larger population and landscape sizes, but the precise connection of these models to forward-time demography is not yet clear. Alternatively, implementation of parallelized calculations may allow progress with forward-time simulations.

Finally, we believe that the difficulties in correcting for population structure in continuous populations using principal components analysis or similar decompositions is a difficult issue, well worth considering on its own. How can we best avoid spurious correlations while correlating genetic and phenotypic variation without underpowering the methods? Perhaps optimistically, we posit that process-driven descriptions of ancestry and/or more generalized unsupervised methods may be able to better account for carry out this task.

## Acknowledgements

We thank Brandon Cooper, Matt Hahn, Doc Edge, and others for reading and thinking about this manuscript. Three anonymous reviewers and the suggestions from editors of GENETICS significantly improved the final manuscript. CJB and ADK were supported by NIH award R01GM117241.

## Literature Cited

- Aguillon, S. M., J. W. Fitzpatrick, R. Bowman, S. J. Schoech, A. G. Clark, *et al.*, 2017 Deconstructing isolation-by-distance: The genomic consequences of limited dispersal. *PLOS Genetics* **13**: 1–27.
- Al-Asadi, H., D. Petkova, M. Stephens, and J. Novembre, 2019 Estimating recent migration and population-size surfaces. *PLoS genetics* **15**: e1007908.
- Allee, W. C., O. Park, A. E. Emerson, T. Park, K. P. Schmidt, *et al.*, 1949 Principles of animal ecology. Technical report, Saunders Company Philadelphia, Pennsylvania, USA.
- Antlfinger, A. E., 1982 Genetic neighborhood structure of the salt marsh composite, *Borrichia frutescens*. *Journal of Heredity* **73**: 128–132.
- Antolin, M. F., B. V. Horne, M. D. Berger, Jr., A. K. Holloway, J. L. Roach, *et al.*, 2001 Effective population size and genetic structure of a piute ground squirrel (*Spermophilus mollis*) population. *Canadian Journal of Zoology* **79**: 26–34.
- Antonovics, J. and D. A. Levin, 1980 The ecological and genetic consequences of density-dependent regulation in plants. *Annual Review of Ecology and Systematics* **11**: 411–452.
- Ashander, J., P. Ralph, E. McCartney-Melstad, and H. B. Shaffer, 2018 Demographic inference in a spatially-explicit ecological model from genomic data: a proof of concept for the mojave desert tortoise. *bioRxiv*.
- Baharian, S., M. Barakatt, C. R. Gignoux, S. Shringarpure, J. Errington, *et al.*, 2016 The great migration and African-American genomic diversity. *PLOS Genetics* **12**: 1–27.
- Barton, N. H., F. Depaulis, and A. M. Etheridge, 2002 Neutral evolution in spatially continuous populations. *Theoretical Population Biology* **61**: 31–48.

- 851 Barton, N. H., J. Kelleher, and A. M. Etheridge, 2010 A new model for extinction and recolonization in  
852 two dimensions: Quantifying phylogeography. *Evolution* **64**: 2701–2715.
- 853 Benjamini, Y. and D. Yekutieli, 2001 The control of the false discovery rate in multiple testing under  
854 dependency. *The Annals of Statistics* **29**: 1165–1188.
- 855 Berg, E. E. and J. L. Hamrick, 1995 Fine-scale genetic structure of a turkey oak forest. *Evolution* **49**:  
856 110–120.
- 857 Berg, J. J., A. Harpak, N. Sinnott-Armstrong, A. M. Joergensen, H. Mostafavi, *et al.*, 2018 Reduced  
858 signal for polygenic adaptation of height in UK Biobank. *bioRxiv*.
- 859 Bolker, B. and S. W. Pacala, 1997 Using moment equations to understand stochastically driven spatial  
860 pattern formation in ecological systems. *Theoretical Population Biology* **52**: 179 – 197.
- 861 Bolker, B. M., S. W. Pacala, and C. Neuhauser, 2003 Spatial dynamics in model plant communities:  
862 What do we really know? *The American Naturalist* **162**: 135–148, PMID: 12858259.
- 863 Browning, S. R. and B. L. Browning, 2015 Accurate non-parametric estimation of recent effective  
864 population size from segments of identity by descent. *The American Journal of Human Genetics* **97**:  
865 404–418.
- 866 Bulik-Sullivan, B. K., P.-R. Loh, H. K. Finucane, S. Ripke, J. Yang, *et al.*, 2015 LD score regression  
867 distinguishes confounding from polygenicity in genome-wide association studies. *Nature Genetics*  
868 **47**: 291 EP –.
- 869 Campbell, D. R. and J. L. Dooley, 1992 The spatial scale of genetic differentiation in a hummingbird-  
870 pollinated plant: Comparison with models of isolation by distance. *The American Naturalist* **139**:  
871 735–748.
- 872 Champer, J., I. Kim, S. E. Champer, A. G. Clark, and P. W. Messer, 2019 Suppression gene drive in  
873 continuous space can result in unstable persistence of both drive and wild-type alleles. *bioRxiv* .
- 874 Chapman, N. H. and E. A. Thompson, 2002 The effect of population history on the lengths of ancestral  
875 chromosome segments. *Genetics* **162**: 449–458.
- 876 Chikhi, L., V. C. Sousa, P. Luisi, B. Goossens, and M. A. Beaumont, 2010 The confounding effects of  
877 population structure, genetic diversity and the sampling scheme on the detection and quantification  
878 of population size changes. *Genetics* **186**: 983–995.
- 879 Crawley, M. J., 1990 The population dynamics of plants. *Philosophical Transactions of the Royal Society  
880 of London. Series B: Biological Sciences* **330**: 125–140.
- 881 Durrett, R. and S. Levin, 1994 The importance of being discrete (and spatial). *Theoretical Population  
882 Biology* **46**: 363–394.
- 883 Eguiarte, L. E., A. Búrquez, J. Rodríguez, M. Martínez-Ramos, J. Sarukhán, *et al.*, 1993 Direct and  
884 indirect estimates of neighborhood and effective population size in a tropical palm, *Astrocaryum  
885 mexicanum*. *Evolution* **47**: 75–87.
- 886 Epperson, B., 2003 *Geographical Genetics*. Monographs in Population Biology, Princeton University  
887 Press.
- 888 Felsenstein, J., 1975 A pain in the torus: Some difficulties with models of isolation by distance. *The  
889 American Naturalist* **109**: 359–368.
- 890 Fournier, N. and S. Méléard, 2004 A microscopic probabilistic description of a locally regulated  
891 population and macroscopic approximations. *The Annals of Applied Probability* **14**: 1880–1919.
- 892 Fox, J. and S. Weisberg, 2011 *An R Companion to Applied Regression*. Sage, Thousand Oaks CA, second  
893 edition.
- 894 Garcia, J. and C. Quintana-Domeque, 2006 The evolution of adult height in Europe: A brief note.  
895 Working Paper .
- 896 Garcia, J. and C. Quintana-Domeque, 2007 The evolution of adult height in Europe: A brief note.  
897 *Economics & Human Biology* **5**: 340 – 349.
- 898 Garud, N. R., P. W. Messer, E. O. Buzbas, and D. A. Petrov, 2015 Recent selective sweeps in North  
899 American *Drosophila melanogaster* show signatures of soft sweeps. *PLOS Genetics* **11**: 1–32.
- 900 Griffiths, R., S. Tavaré, *et al.*, 1999 The ages of mutations in gene trees. *The Annals of Applied Probability*  
901 **9**: 567–590.
- 902 Guindon, S., H. Guo, and D. Welch, 2016 Demographic inference under the coalescent in a spatial  
903 continuum. *Theoretical population biology* **111**: 43–50.

- 904 Haller, B. C., J. Galloway, J. Kelleher, P. W. Messer, and P. L. Ralph, 2019 Tree-sequence recording  
 905 in SLiM opens new horizons for forward-time simulation of whole genomes. *Molecular Ecology*  
 906 Resources **19**: 552–566.
- 907 Haller, B. C. and P. W. Messer, 2019 SLiM 3: Forward genetic simulations beyond the Wright–Fisher  
 908 model. *Molecular biology and evolution* **36**: 632–637.
- 909 Harris, K. and R. Nielsen, 2013 Inferring demographic history from a spectrum of shared haplotype  
 910 lengths. *PLOS Genetics* **9**: 1–20.
- 911 Haworth, S., R. Mitchell, L. Corbin, K. H. Wade, T. Dudding, *et al.*, 2019 Apparent latent structure within  
 912 the UK Biobank sample has implications for epidemiological analysis. *Nature communications* **10**:  
 913 333.
- 914 Huillet, T. and M. Möhle, 2011 On the extended Moran model and its relation to coalescents with  
 915 multiple collisions. *Theoretical Population Biology* pp. –.
- 916 International Schizophrenia Consortium *et al.*, 2009 Common polygenic variation contributes to risk of  
 917 schizophrenia and bipolar disorder. *Nature* **460**: 748.
- 918 Jackson, N. D. and L. Fahrig, 2014 Landscape context affects genetic diversity at a much larger spatial  
 919 extent than population abundance. *Ecology* **95**: 871–881.
- 920 Jasper, M., T. Schmidt, N. Ahmad, S. Sinkins, and A. Hoffmann, 2019 A genomic approach to inferring  
 921 kinship reveals limited intergenerational dispersal in the yellow fever mosquito. *bioRxiv* .
- 922 Jay, F., P. Sjödin, M. Jakobsson, and M. G. Blum, 2012 Anisotropic isolation by distance: The main  
 923 orientations of human genetic differentiation. *Molecular Biology and Evolution* **30**: 513–525.
- 924 Kang, H. M., J. H. Sul, S. K. Service, N. A. Zaitlen, S.-y. Kong, *et al.*, 2010 Variance component model to  
 925 account for sample structure in genome-wide association studies. *Nature Genetics* **42**: 348 EP –.
- 926 Kang, H. M., N. A. Zaitlen, C. M. Wade, A. Kirby, D. Heckerman, *et al.*, 2008 Efficient control of  
 927 population structure in model organism association mapping. *Genetics* **178**: 1709–1723.
- 928 Kelleher, J., A. Etheridge, and N. Barton, 2014 Coalescent simulation in continuous space: Algorithms  
 929 for large neighbourhood size. *Theoretical Population Biology* **95**: 13 – 23.
- 930 Kelleher, J., A. M. Etheridge, and G. McVean, 2016 Efficient coalescent simulation and genealogical  
 931 analysis for large sample sizes. *PLoS Comput Biol* **12**: 1–22.
- 932 Kelleher, J., K. R. Thornton, J. Ashander, and P. L. Ralph, 2018 Efficient pedigree recording for fast  
 933 population genetics simulation. *PLOS Computational Biology* **14**: 1–21.
- 934 Kerster, H. W., 1964 Neighborhood size in the rusty lizard, *Sceloporus olivaceus*. *Evolution* **18**: 445–457.
- 935 Kingman, J., 1982 The coalescent. *Stochastic Processes and their Applications* **13**: 235 – 248.
- 936 Law, R., D. J. Murrell, and U. Dieckmann, 2003 Population growth in space and time: Spatial logistic  
 937 equations. *Ecology* **84**: 252–262.
- 938 Lawson, D. J., N. M. Davies, S. Haworth, B. Ashraf, L. Howe, *et al.*, 2019 Is population structure in the  
 939 genetic biobank era irrelevant, a challenge, or an opportunity? *Human Genetics* .
- 940 Leblois, R., A. Estoup, and R. Streiff, 2006 Genetics of recent habitat contraction and reduction in  
 941 population size: does isolation by distance matter? *Molecular Ecology* **15**: 3601–3615.
- 942 Liu, X. and Y.-X. Fu, 2015 Exploring population size changes using SNP frequency spectra. *Nature*  
 943 Genetics **47**: 555 EP –.
- 944 Lloyd, M., 1967 ‘Mean crowding’. *Journal of Animal Ecology* **36**: 1–30.
- 945 Lundgren, E. and P. L. Ralph, 2019 Are populations like a circuit? Comparing isolation by resistance to  
 946 a new coalescent-based method. *Molecular Ecology Resources* **19**: 1388–1406.
- 947 Martin, A. R., M. Kanai, Y. Kamatani, Y. Okada, B. M. Neale, *et al.*, 2019 Clinical use of current polygenic  
 948 risk scores may exacerbate health disparities. *Nature Genetics* **51**: 584–591.
- 949 Maruyama, T., 1972 Rate of decrease of genetic variability in a two-dimensional continuous population  
 950 of finite size. *Genetics* **70**: 639–651.
- 951 Mathieson, I. and G. McVean, 2012 Differential confounding of rare and common variants in spatially  
 952 structured populations. *Nature Genetics* **44**: 243 EP –.
- 953 Mazet, O., W. Rodríguez, S. Grusea, S. Boitard, and L. Chikhi, 2015 On the importance of being  
 954 structured: instantaneous coalescence rates and human evolution—lessons for ancestral population  
 955 size inference? *Heredity* **116**: 362 EP –.
- 956 Miles, A. and N. Harding, 2017 *cgh/scikit-allel*: v1.1.8.

- 957 Neel, M. C., K. McKelvey, N. Ryman, M. W. Lloyd, R. Short Bull, *et al.*, 2013 Estimation of effective  
958 population size in continuously distributed populations: there goes the neighborhood. *Heredity* **111**:  
959 189 EP –.
- 960 Novembre, J. and M. Slatkin, 2009 Likelihood-based inference in isolation-by-distance models using  
961 the spatial distribution of low-frequency alleles. *Evolution* **63**: 2914–2925.
- 962 Pamilo, P., 1983 Genetic differentiation within subdivided populations of formica ants. *Evolution* **37**:  
963 1010–1022.
- 964 Patterson, N., A. L. Price, and D. Reich, 2006 Population structure and eigenanalysis. *PLOS Genetics* **2**:  
965 1–20.
- 966 Petkova, D., J. Novembre, and M. Stephens, 2015 Visualizing spatial population structure with esti-  
967 mated effective migration surfaces. *Nature Genetics* **48**: 94 EP –.
- 968 Price, A. L., N. J. Patterson, R. M. Plenge, M. E. Weinblatt, N. A. Shadick, *et al.*, 2006 Principal  
969 components analysis corrects for stratification in genome-wide association studies. *Nature Genetics*  
970 **38**: 904 EP –.
- 971 Pritchard, J. K., M. Stephens, and P. Donnelly, 2000 Inference of population structure using multilocus  
972 genotype data. *Genetics* **155**: 945–959.
- 973 Ptak, S. E. and M. Przeworski, 2002 Evidence for population growth in humans is confounded by  
974 fine-scale population structure. *Trends in Genetics* **18**: 559–563.
- 975 Purcell, S., B. Neale, K. Todd-Brown, L. Thomas, M. A. Ferreira, *et al.*, 2007 Plink: A tool set for  
976 whole-genome association and population-based linkage analyses. *The American Journal of Human  
977 Genetics* **81**: 559 – 575.
- 978 R Core Team, 2018 *R: A Language and Environment for Statistical Computing*. R Foundation for Statistical  
979 Computing, Vienna, Austria.
- 980 Ralph, P. and G. Coop, 2013 The geography of recent genetic ancestry across Europe. *PLoS Biol* **11**:  
981 e1001555.
- 982 Ralph, P., J. Kelleher, J. Galloway, , and J. Ashander, 2019a pyslim.
- 983 Ralph, P., K. Thornton, and J. Kelleher, 2019b Efficiently summarizing relationships in large samples: a  
984 general duality between statistics of genealogies and genomes. *bioRxiv* .
- 985 Ringbauer, H., G. Coop, and N. H. Barton, 2017 Inferring recent demography from isolation by distance  
986 of long shared sequence blocks. *Genetics* **205**: 1335–1351.
- 987 Robledo-Arnuncio, J. J. and F. Rousset, 2010 Isolation by distance in a continuous population under  
988 stochastic demographic fluctuations. *Journal of Evolutionary Biology* **23**: 53–71.
- 989 Rossine, F. W. S., 2014 *Espaço e diversificação: uma perspectiva teórica*. Master's dissertation in ecologia:  
990 Ecossistemas terrestres e aquáticos, University of São Paulo, São Paulo : Instituto de Biociências.
- 991 Rousset, F., 1997 Genetic differentiation and estimation of gene flow from F-statistics under isolation  
992 by distance. *Genetics* **145**: 1219–1228.
- 993 Rousset, F. and R. Leblois, 2011 Likelihood-based inferences under isolation by distance: Two-  
994 dimensional habitats and confidence intervals. *Molecular Biology and Evolution* **29**: 957–973.
- 995 Sawyer, S., 1977 On the past history of an allele now known to have frequency p. *Journal of Applied  
996 Probability* **14**: 439–450.
- 997 Schiffels, S. and R. Durbin, 2014 Inferring human population size and separation history from multiple  
998 genome sequences. *Nature Genetics* **46**: 919 EP –.
- 999 Schrider, D. R. and A. D. Kern, 2018 Supervised machine learning for population genetics: A new  
1000 paradigm. *Trends in Genetics* **34**: 301 – 312.
- 1001 Sharbel, T. F., B. Haubold, and T. Mitchell-Olds, 2000 Genetic isolation by distance in *Arabidopsis  
1002 thaliana*: biogeography and postglacial colonization of Europe. *Molecular Ecology* **9**: 2109–2118.
- 1003 Sheehan, S., K. Harris, and Y. S. Song, 2013 Estimating variable effective population sizes from multiple  
1004 genomes: A sequentially Markov conditional sampling distribution approach. *Genetics* **194**: 647–662.
- 1005 Shirk, A. J. and S. A. Cushman, 2014 Spatially-explicit estimation of Wright's neighborhood size in  
1006 continuous populations. *Frontiers in Ecology and Evolution* **2**: 62.
- 1007 Slatkin, M. and N. H. Barton, 1989 A comparison of three indirect methods for estimating average  
1008 levels of gene flow. *Evolution* **43**: 1349–1368.
- 1009 Sohail, M., R. M. Maier, A. Ganna, A. Bloemendal, A. R. Martin, *et al.*, 2018 Signals of polygenic

- adaptation on height have been overestimated due to uncorrected population structure in genome-wide association studies. *bioRxiv*.
- St. Onge, K. R., A. E. Palmé, S. I. Wright, and M. Lascoux, 2012 Impact of sampling schemes on demographic inference: An empirical study in two species with different mating systems and demographic histories. *G3: Genes, Genomes, Genetics* **2**: 803–814.
- Städler, T., B. Haubold, C. Merino, W. Stephan, and P. Pfaffelhuber, 2009 The impact of sampling schemes on the site frequency spectrum in nonequilibrium subdivided populations. *Genetics* **182**: 205–216.
- Tajima, F., 1989 Statistical method for testing the neutral mutation hypothesis by DNA polymorphism. *Genetics* **123**: 585–595.
- Terhorst, J., J. A. Kamm, and Y. S. Song, 2016 Robust and scalable inference of population history from hundreds of unphased whole genomes. *Nature Genetics* **49**: 303 EP –.
- Turchin, M. C., C. W. Chiang, C. D. Palmer, S. Sankararaman, D. Reich, *et al.*, 2012 Evidence of widespread selection on standing variation in Europe at height-associated SNPs. *Nature Genetics* **44**: 1015 EP –.
- Wahlund, S., 1928 Zusammensetzung von populationen und korrelationserscheinungen vom standpunkt der vererbungslehre aus betrachtet. *Hereditas* **11**: 65–106.
- Wakeley, J., 1999 Nonequilibrium migration in human history. *Genetics* **153**: 1863–1871.
- Wakeley, J., 2009 *Coalescent Theory, an Introduction*. Roberts and Company, Greenwood Village, CO.
- Wakeley, J. and T. Takahashi, 2003 Gene genealogies when the sample size exceeds the effective size of the population. *Mol Biol Evol* **20**: 208–213.
- Wickham, H., 2016 *ggplot2: Elegant Graphics for Data Analysis*. Springer-Verlag New York.
- Wilke, C. O., 2019 *cowplot: Streamlined Plot Theme and Plot Annotations for 'ggplot2'*. R package version 0.9.4.
- Wilkins, J. F., 2004 A separation-of-timescales approach to the coalescent in a continuous population. *Genetics* **168**: 2227–2244.
- Wilkins, J. F. and J. Wakeley, 2002 The coalescent in a continuous, finite, linear population. *Genetics* **161**: 873–888.
- Wray, N. R., M. E. Goddard, and P. M. Visscher, 2007 Prediction of individual genetic risk to disease from genome-wide association studies. *Genome research* **17**: 1520–1528.
- Wright, S., 1931 Evolution in Mendelian populations. *Genetics* **16**: 97.
- Wright, S., 1943 Isolation by distance. *Genetics* **28**: 114–138.
- Wright, S., 1946 Isolation by distance under diverse systems of mating. *Genetics* **31**: 336.
- Young, A. I., M. L. Frigge, D. F. Gudbjartsson, G. Thorleifsson, G. Bjornsdottir, *et al.*, 2018 Relatedness disequilibrium regression estimates heritability without environmental bias. *Nature Genetics* **50**: 1304–1310.
- Young, H. J., 1988 Neighborhood size in a beetle pollinated tropical aroid: effects of low density and asynchronous flowering. *Oecologia* **76**: 461–466.
- Yu, J., G. Pressoir, W. H. Briggs, I. Vroh Bi, M. Yamasaki, *et al.*, 2005 A unified mixed-model method for association mapping that accounts for multiple levels of relatedness. *Nature Genetics* **38**: 203 EP –.
- Zähle, I., J. T. Cox, and R. Durrett, 2005 The stepping stone model. II. Genealogies and the infinite sites model. *Ann. Appl. Probab.* **15**: 671–699.

1052     **Appendix 1**

1053     **Comparisons with Stepping-Stone Models**

1054     We also compared our model results to a regular grid of discrete populations, which is commonly used  
 1055     as an approximation of continuous geography. An important reason that this approximation is often  
 1056     made is that it allows more efficient, coalescent simulations; we implemented these using `msprime`  
 1057     (Kelleher *et al.* 2016). In this class of models we imagine an  $n \times n$  grid of populations exchanging  
 1058     migrants with neighboring populations at rate  $m$ . If these models are good approximations of the  
 1059     continuous case we expect that results will converge as  $n \rightarrow \infty$  (while scaling  $m$  appropriately and  
 1060     keeping total population size fixed), so we ran simulations while varying  $n$  from 5 to 50 (Table  
 1061     A1). To compare with continuous models we first distributed the same “effective” number of  
 1062     individuals across the landscape as in our continuous-space simulations ( $\approx 6100$ , estimated from  $\theta_\pi$   
 1063     of random-mating continuous-space simulations). We then approximate the mean per-generation  
 1064     dispersal distance  $\sigma$  given a total landscape width  $W$  as the product of the probability of an individual  
 1065     being a migrant and the distance traveled by migrants:  $\sigma = 4m(W/n)$ . This means that  $m$  in different  
 1066     simulations with the same  $\sigma$  scales with  $\sqrt{n}$ . We ran 500 simulations for each value of  $n$  while  
 1067     sampling  $\sigma$  from  $U(0.2, 4)$ . We then randomly selected 60 diploid individuals from each simulation  
 1068     (approximating diploidy by combining pairs of chromosomes with contiguous indices within demes)  
 1069     and calculated a set of six summary statistics using the scripts described in the summary statistics  
 1070     portion of the main text.

demes per side ( $n$ )	$N_e$ per deme	samples per deme
5	244	20
10	61	10
20	15.25	2
50	2.44	1

**Table A1** stepping-stone simulation parameters

1071     In general we find many of the qualitative trends are similar among continuous and stepping-  
 1072     stone models and that, at low neighborhood sizes, many (but not all) statistics from stepping-stone  
 1073     models approach the continuous model as the resolution of the grid increases. For example,  $\theta_\pi$  is  
 1074     lower in stepping-stone models at low neighborhood sizes (i.e., low  $m$ ), but increases to approach the  
 1075     continuous case as the resolution of the landscape increases. Similar patterns are observed for observed  
 1076     heterozygosity. However,  $\theta_W$  behaves differently, showing a non-monotonic relationship with grid  
 1077     resolution. This results in an increasingly positive Tajima’s  $D$  in grid simulations at small neighborhood  
 1078     sizes, to a much greater extent than seen in a continuous model. In contrast to  $\theta_\pi$ , increasing the  
 1079     resolution of the grid causes Tajima’s  $D$  to deviate *more* from what is seen in the continuous model.  
 1080     Similarly, although  $F_{IS}$  approaches the continuous case as the resolution of the grid increases at  
 1081     very small neighborhood sizes, at intermediate neighborhood sizes the continuous case best matches  
 1082     intermediate grid resolutions.

1083     These differences relative to our continuous model mainly reflect two shortcomings of the reverse-  
 1084     time stepping stone model. If we simulate a coarse grid with relatively large populations in each  
 1085     deme, we cannot accurately capture the dynamics of small neighborhood sizes because mating within  
 1086     each deme remains random regardless of the migration rate connecting demes. This likely explains  
 1087     the trends in  $\theta_\pi$ , observed heterozygosity, and  $F_{IS}$ . However increasing the number of demes while  
 1088     holding the total number of individuals constant results in small within-deme populations for which  
 1089     even the minimum sample size of 1 approaches the local  $N_e$  (Table A1). This results in an excess  
 1090     of short terminal branches in the coalescent tree, which decreases the total branch length and leads  
 1091     to fewer segregating sites, deflated  $\theta_W$ , and inflated Tajima’s  $D$ . Overall, the stepping-stone model  
 1092     reproduces important features of spatial structure in our continuous space model, such as a decline in

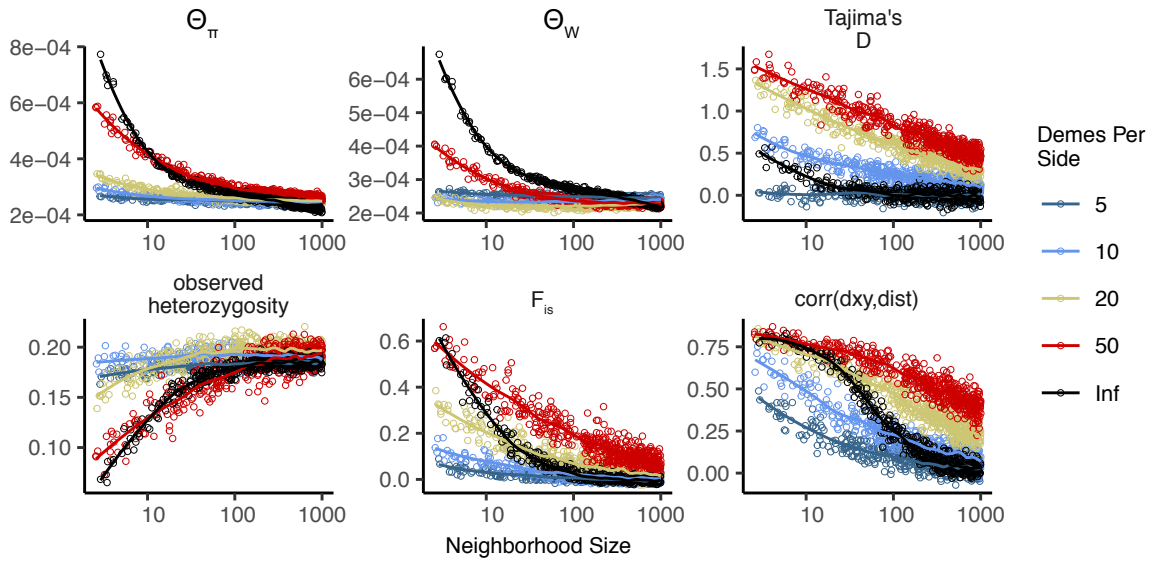


**Figure A1** Summary statistics for 2-dimensional coalescent stepping-stone models with fixed total  $N_e$  and varying numbers of demes per side. The black “infinite” points are from our forward-time continuous space model. Inter-deme migration rates are related to  $\sigma$  as described above.

1093  $\theta_\pi$  and correlations between spatial and genetic distance with increasing migration, but introduces  
1094 artifacts caused by binning the landscape into discrete demes.

1095 **Demographic model**

1096 Local population regulation is controlled by two parameters,  $L$ , and  $K$ . Here, we show that these  
1097 should be close to the average lifespan of an individual and the average number of individuals per  
1098 unit area, respectively. We chose our demographic model so that every individual has on average  $1/L$   
1099 offspring each time step, and if the local population density of an individual is  $n$ , then their probability  
1100 of survival until the next time step is (equation (1)):

$$p = \min \left( 0.95, \frac{1}{1 + n/(K(1+L))} \right). \quad (3)$$

1101 We capped survival at 0.95 so that we would not have exceptionally long-lived individuals in sparsely  
1102 populated areas – otherwise, an isolated individual might live for a very long time. Since  $1 - p \approx$   
1103  $n/(K(1+L))$ , mortality goes up roughly linearly with the number of neighbors (on a scale given by  
1104  $K$ ), as would be obtained if, for instance, mortality is due to agonistic interactions. Ignoring migration,  
1105 a region is at demographic equilibrium if the per-capita probability of death is equal to the birth rate,  
1106 i.e., if  $1 - p = 1/L$ . (Note that there is no effect of age in the model, which would make the analysis  
1107 more complicated.) Solving this for  $n$ , we get that in a well-mixed population, the equilibrium density  
1108 should be around

$$n = K \frac{L+1}{L-1} \quad (4)$$

1109 individuals per unit area. At this density, the per-capita death rate is  $1/L$ , so the mean lifetime is  $L$ .  
1110 This equilibrium density is *not*  $K$ , but (since  $L = 4$ ) is two-thirds larger. However, in practice this model  
1111 leads to a total population size which is around  $K$  multiplied by total geographic area (but which  
1112 depends on  $\sigma$ , as discussed above). The main reason for this is that since offspring tend to be near  
1113 their parents, individuals tend to be “clumped”, and so experience a higher average density than the  
1114 “density” one would compute by dividing census size by geographic area (Lloyd 1967). To maintain a

<sup>1115</sup> constant expected total population size would require making (say)  $K$  depend on  $\sigma$ ; however, typical  
<sup>1116</sup> local population densities might then be more dissimilar.

<sup>1117</sup> **Supplementary Figures and Tables**

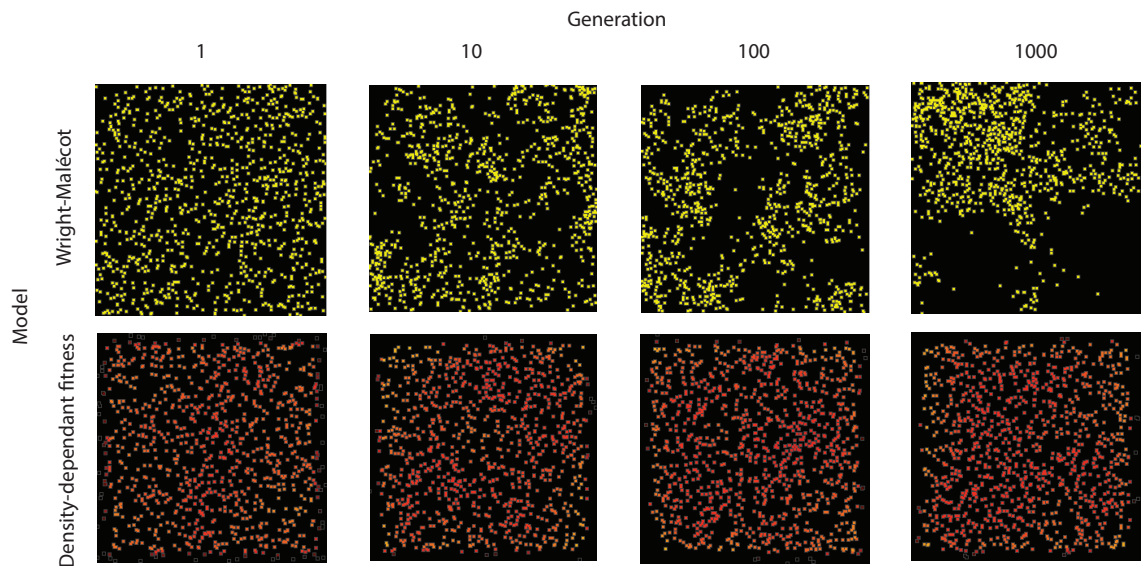


**Figure S1** Maps of individual locations in a continuous-space Wright-Malécot model with independent dispersal of all individuals (top) and under our continuous space model incorporating density-dependant fitness (bottom). The clustering seen in the top row is the “Pain in the Torus” described by Felsenstein (1975).

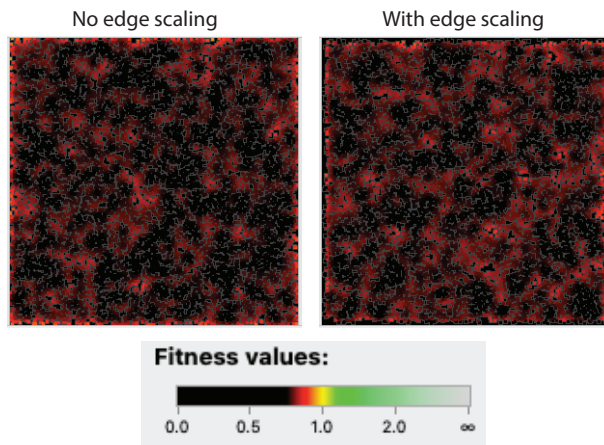


**Figure S2** Comparison of individual fitness across the landscape in simulations with (right) and without (left) a decline in fitness approaching range edges. Note the slight excess of high-fitness individuals at edges on the left, which is (partially) counteracted by the scaling procedure.

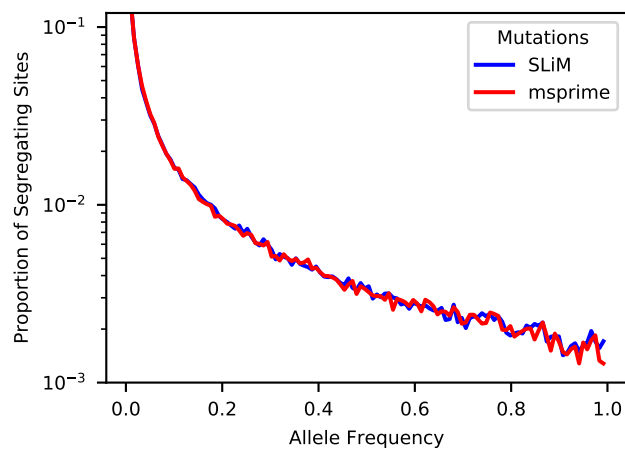


**Figure S3** Site frequency spectra from a simulation with neighborhood size = 12.5 when mutations are recorded directly in SLiM (blue line) or applied later in msprime (red line).

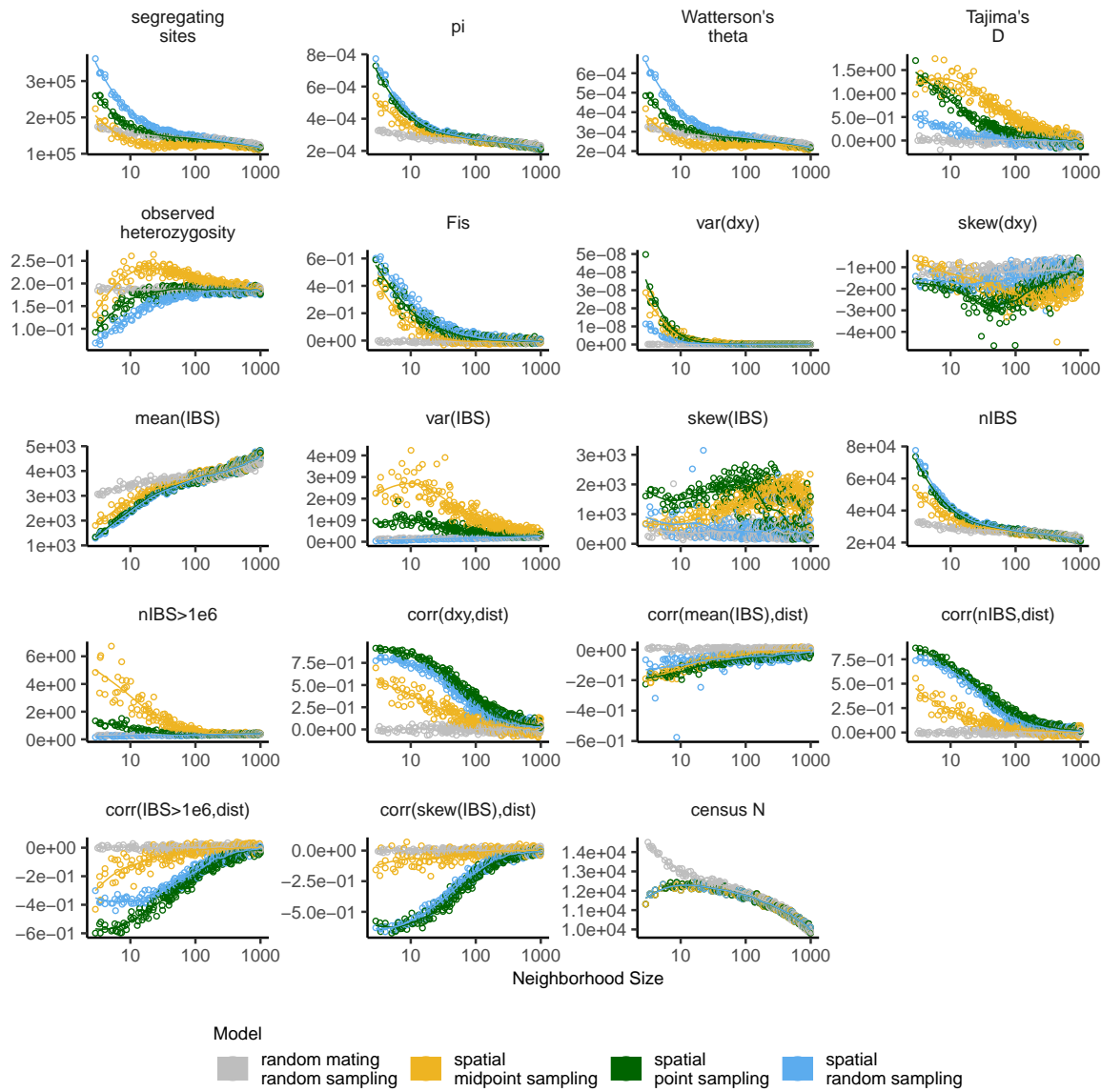


**Figure S4** Change in summary statistics by neighborhood size and sampling scheme calculated from simulated sequence data of 60 individuals.

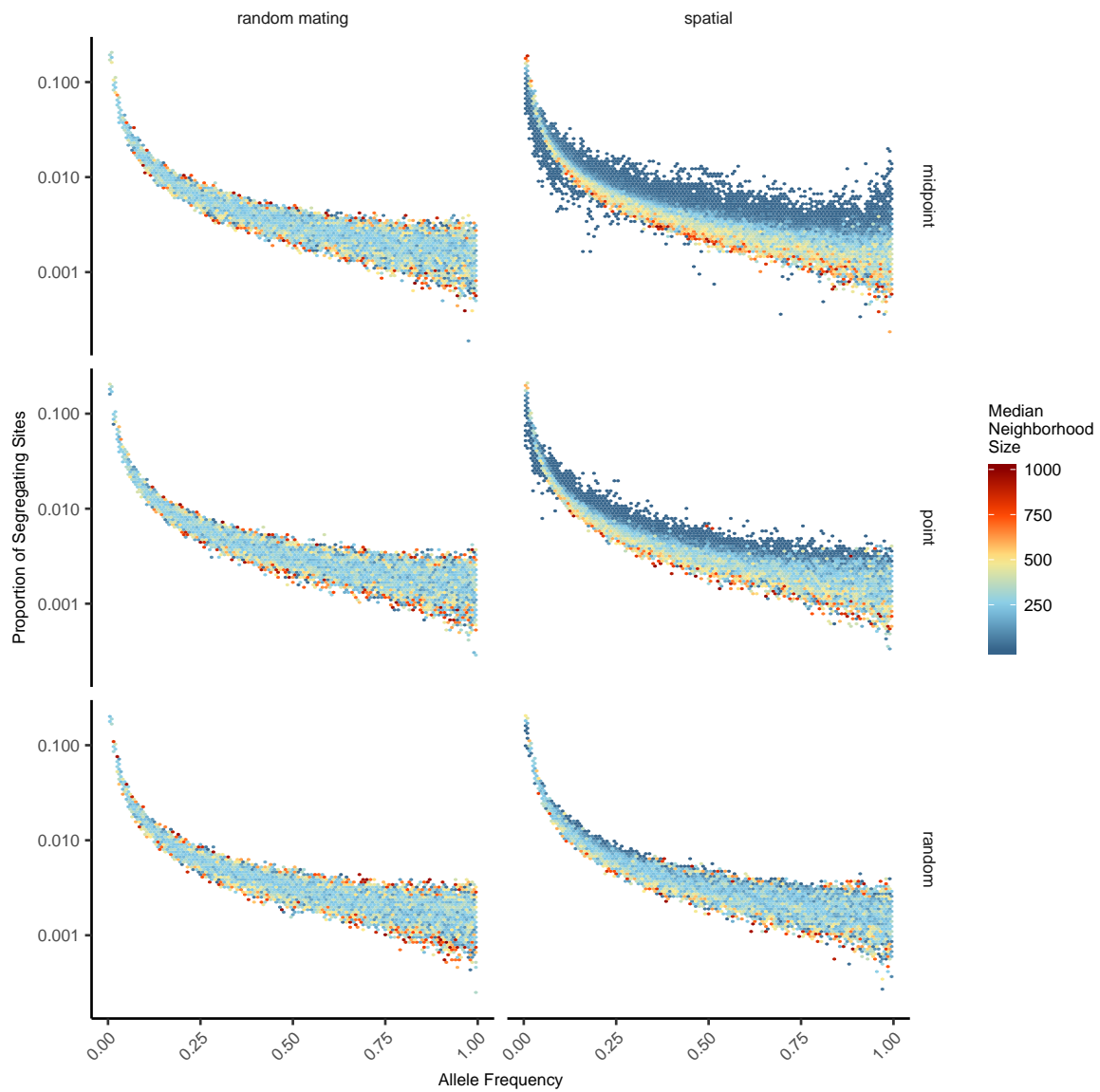


**Figure S5** Site frequency spectra for random mating and spatial SLiM models under all sampling schemes.

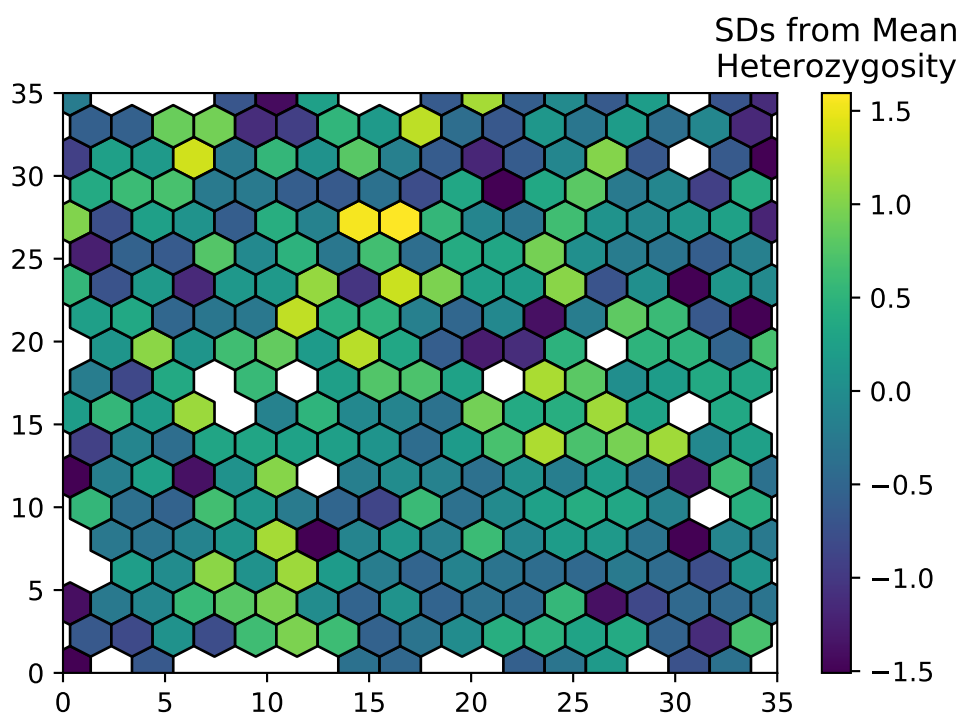


**Figure S6** Variation in observed heterozygosity (i.e. proportion of heterozygous individuals) in hexagonal bins across the landscape, estimated from a random sample of 200 individuals from the final generation of a simulation with neighborhood size  $\approx 25$ . Values were Z-normalized for plotting.

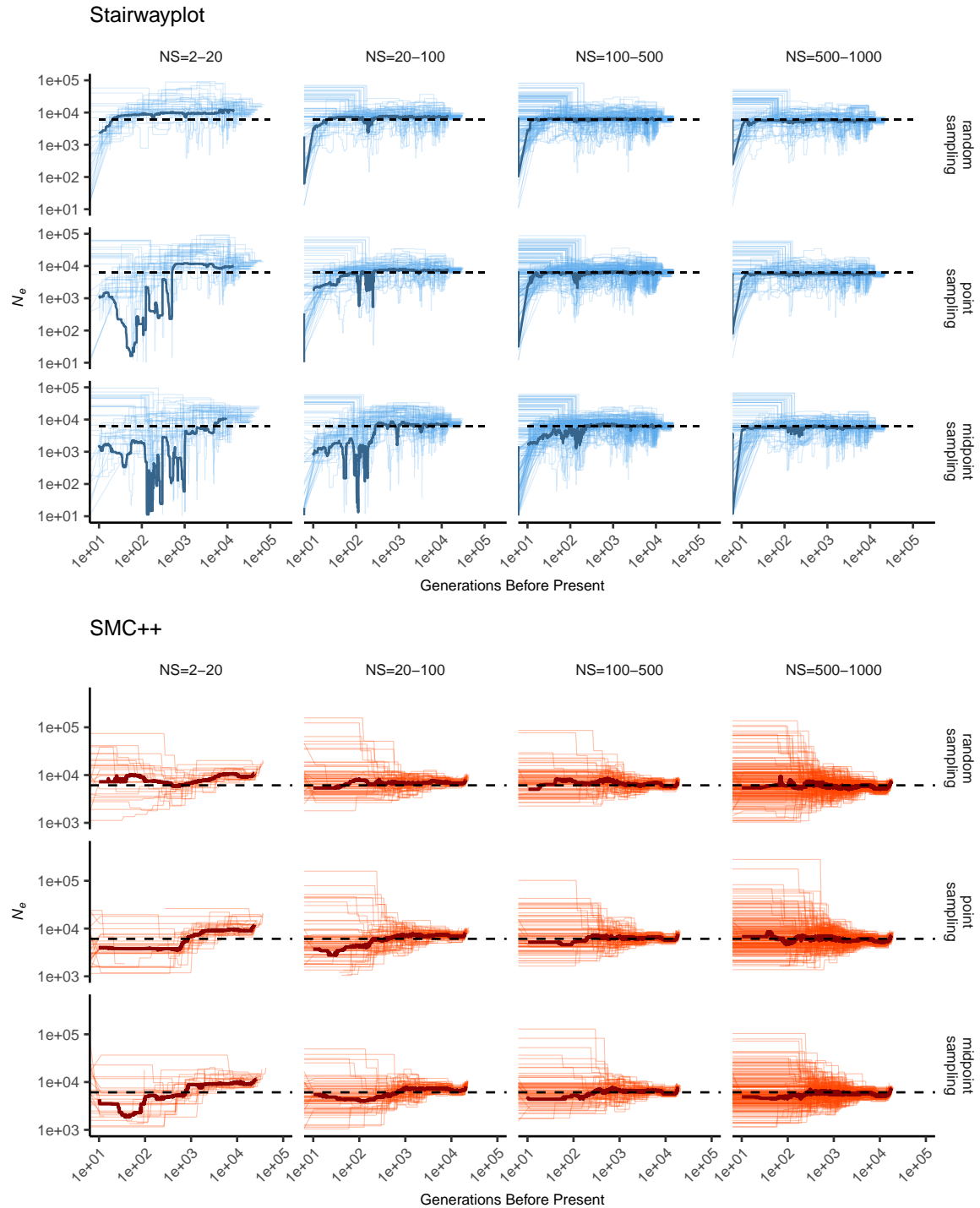


**Figure S7** Inferred demographic histories for spatial SLiM simulations, by sampling scheme and neighborhood size (NS) range. Thick lines are rolling medians across all simulations in a bin and thin lines are best fit models for each simulation. Dashed horizontal lines are the average  $N_e$  across random-mating SLiM models estimated from  $\theta_\pi$ .

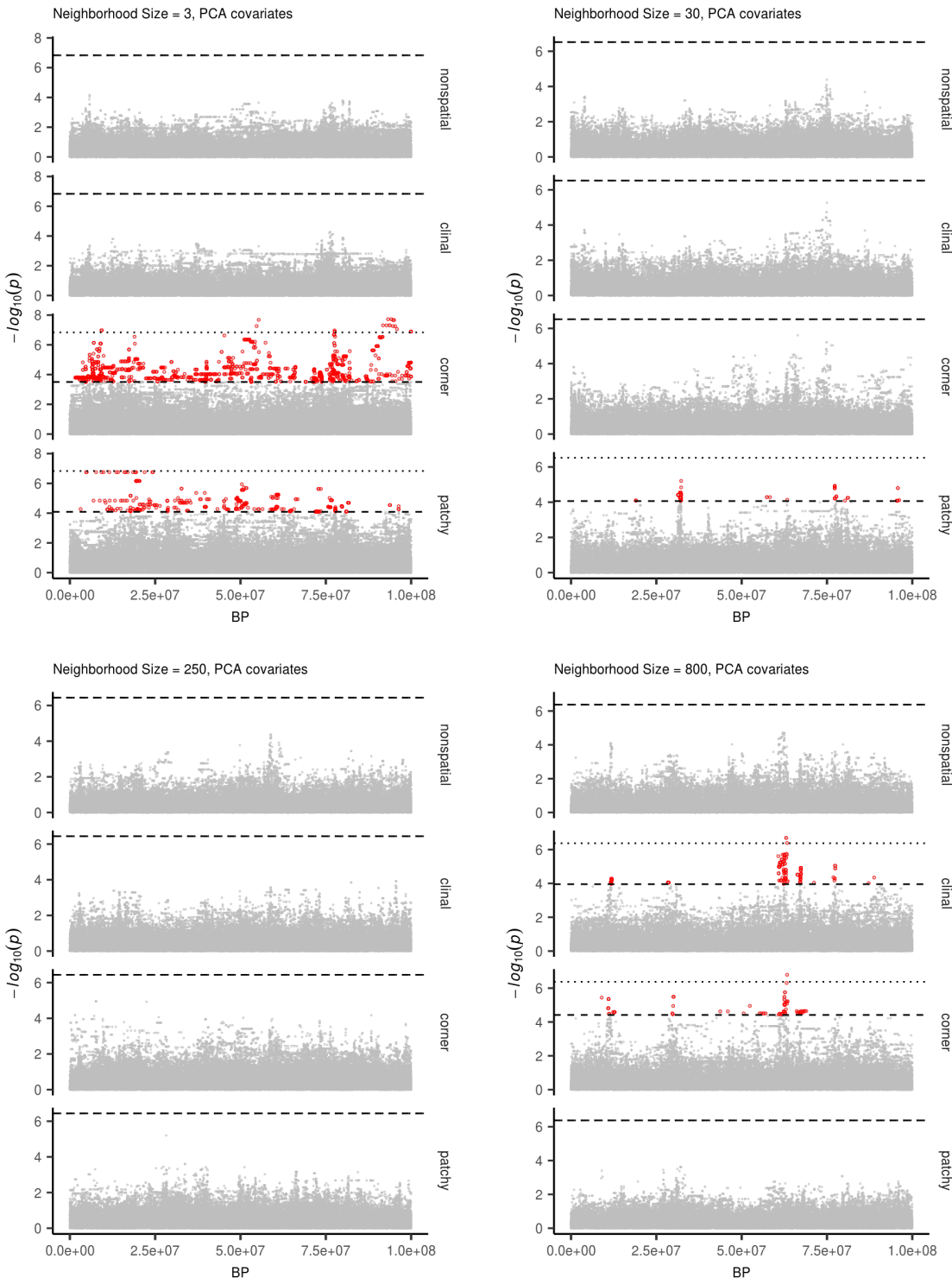


**Figure S8** Manhattan plots for a sample of simulations at varying neighborhood sizes. Labels on the right of each plot describes the spatial distribution of environmental factors (described in the methods section of the main text). Points in red are significantly associated with a nongenetic phenotype using a 5% FDR threshold (dashed line). For runs with significant associations the dotted line is a Bonferroni-adjusted cutoff for  $p = 0.05$ .

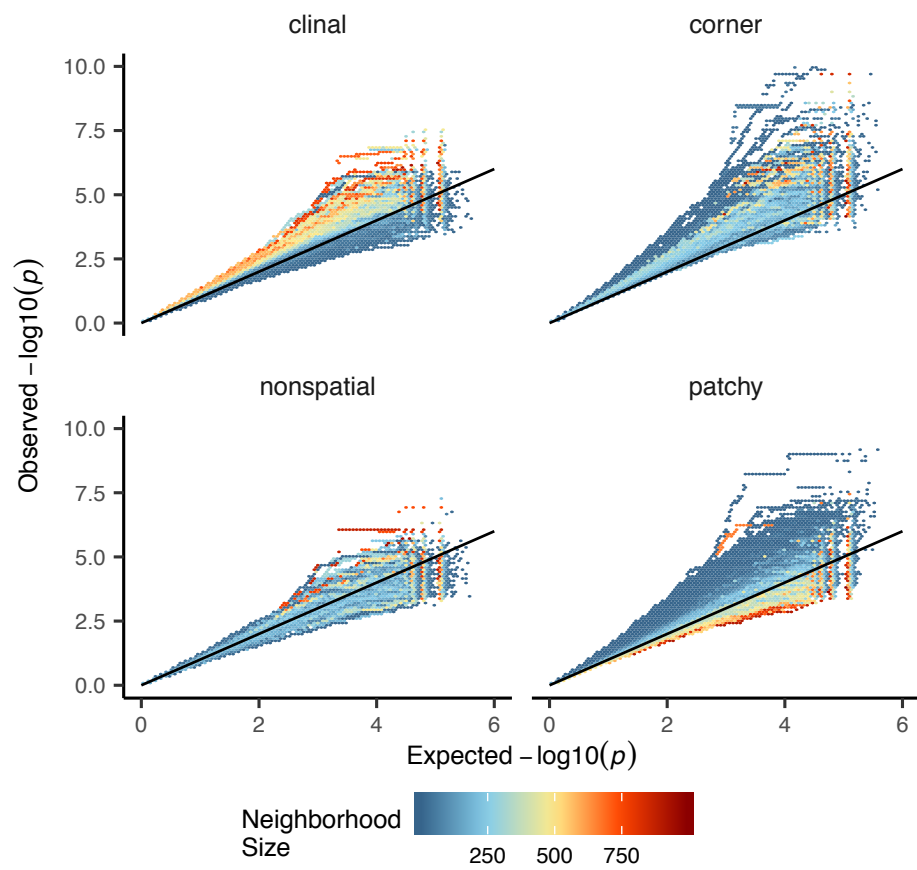


**Figure S9** Quantile-quantile plots showing observed  $-\log_{10}(p)$  for PC-corrected GWAS run on simulations with varying neighborhood sizes and environmental distributions. Hexagonal bins are colored by the average neighborhood size of simulations with points falling in a given region of quantile-quantile space. Qqplots for a subset of these simulations are shown as lines in Figure 8D.

**Table S1** Summary statistics calculated on simulated genotypes.

Statistic	Description
$\Theta_{pi}$	Mean of the distribution of pairwise genetic differences
$\Theta_W$	Effective population size based on segregating sites
Segregating Sites	Total number of segregating sites in the sample
Tajima's $D$	Difference in $\Theta_{pi}$ and $\Theta_W$ over its standard deviation
Observed Heterozygosity	Proportion of heterozygous individuals in the sample
$F_{IS}$	Wright's inbreeding coefficient $1 - H_e / H_o$
$var(D_{xy})$	Variance in the distribution of pairwise genetic distances
$skew(D_{xy})$	Skew of the distribution of pairwise genetic distances
$mean(IVS)$	Mean of the distribution of pairwise identical-by-state (IBS) tract lengths taken over all pairs.
$var(IVS)$	Variance of the distribution of pairwise identical-by-state (IBS) tract lengths taken over all pairs.
$skew(IVS)$	Skew of the distribution of pairwise identical-by-state (IBS) tract lengths taken over all pairs.
$nIBS$	Mean number of IBS tracts with length > 2bp across all pairs in the sample.
$nIBS > 1e6$	Mean number of IBS tracts over $1 \times 10^6$ bp per pair across all pairs in the sample.
$corr(D_{xy}, dist)$	Pearson correlation between genetic distance and $\log_{10}(spatial\ distance)$
$corr(mean(IVS), dist)$	Pearson correlation between the mean of the IBS tract distribution for each pair of samples and $\log_{10}(spatial\ distance)$
$corr(nIBS, dist)$	Pearson correlation between the number of IBS tracts for each pair of samples and $\log_{10}(spatial\ distance)$
$corr(IVS > 1e6, dist)$	Pearson correlation between the number of IBS tracts > $1 \times 10^6$ bp for each pair of samples and $\log_{10}(spatial\ distance)$
$corr(skew(IVS), dist)$	Pearson correlation between the skew of the distribution of pairwise haplotype block lengths for each pair of samples and $\log_{10}(spatial\ distance)$

**Table S2 Anova and Levene's test  $p$  values for differences by sampling strategy. Bolded values are rejected at  $\alpha = 0.05$**

variable	model	p(equal means)	p(equal variance)
segsites	random mating	0.998190	0.980730
$\Theta\pi$	random mating	0.997750	0.996450
$\Theta_W$	random mating	0.998190	0.980730
Tajima's $D$	random mating	0.879690	0.188770
observed heterozygosity	random mating	0.531540	0.433230
$F_{IS}$	random mating	0.474790	0.785730
$mean(D_{xy})$	random mating	0.997770	0.996510
$var(D_{xy})$	random mating	0.283630	0.647240
$skew(D_{xy})$	random mating	0.958320	0.260750
$corr(D_{xy}, dist)$	random mating	0.601980	0.000000
$mean(IBS)$	random mating	0.997960	0.997730
$var(IBS)$	random mating	0.486450	0.399490
$skew(IBS)$	random mating	0.117980	0.069770
$nIBS$	random mating	0.997680	0.996570
$nIBS > 1e6$	random mating	0.834870	0.888730
$corr(mean(IBS), dist)$	random mating	0.073270	0.308420
$corr(IBS > 1e6, dist)$	random mating	0.268440	0.002100
$corr(skew(IBS), dist)$	random mating	0.396920	0.000620
$corr(nIBS, dist)$	random mating	0.581090	0.000000
segsites	spatial	0.000000	0.000000
$\Theta\pi$	spatial	0.026510	0.013440
$\Theta_W$	spatial	0.000000	0.000000
Tajima's $D$	spatial	0.000000	0.000000
observed heterozygosity	spatial	0.000000	0.000000
$F_{IS}$	spatial	0.000000	0.000120
$mean(D_{xy})$	spatial	0.025390	0.012910
$var(D_{xy})$	spatial	0.004970	0.006230
$skew(D_{xy})$	spatial	0.000000	0.000000
$corr(D_{xy}, dist)$	spatial	0.000000	0.000000
$mean(IBS)$	spatial	0.272400	0.114250
$var(IBS)$	spatial	0.000000	0.000000
$skew(IBS)$	spatial	0.000000	0.000000
$nIBS$	spatial	0.033920	0.016640
$nIBS > 1e6$	spatial	0.000000	0.000000
$corr(mean(IBS), dist)$	spatial	0.000000	0.590540
$corr(IBS > 1e6, dist)$	spatial	0.000000	0.000000
$corr(skew(IBS), dist)$	spatial	0.000000	0.000000
$corr(nIBS, dist)$	spatial	0.000000	0.000000